Geological Society of America
Special Paper 415
2006

Using in situ–produced ^{10}Be to quantify active tectonics in the Gurvan Bogd mountain range (Gobi-Altay, Mongolia)

J.-F. Ritz†
R. Vassallo
Laboratoire Dynamique de la Lithosphère, CNRS-UMII UMR 5573, Université Montpellier II, Montpellier, France

R. Braucher
CEREGE, Europole Méditerranéen de l'Arbois, Aix-en-Provence, France

E.T. Brown
Large Lakes Observatory, University of Minnesota, Duluth, Minnesota 55812, USA

S. Carretier
Laboratoire des Mécanismes de Transfert en Géologie, IRD-CNRS-UNIV UMR 5563, Toulouse, France

D.L. Bourlès
CEREGE, Europole Méditerranéen de l'Arbois, Aix-en-Provence, France

ABSTRACT

This paper presents an updated synthesis of morphotectonic studies that quantify active tectonics along the Gurvan Bogd mountain range in the Mongolian Gobi-Altay, the site of one of the strongest historic intracontinental earthquakes (Mw 8.1) in 1957. Our goal was to determine the slip rate along the constituent fault segments and to estimate the return period of such large events. Along each segment, cumulative offsets were estimated from topographic surveys, and the ages of the offset markers were determined using cosmic-ray exposure dating. In this review, we reevaluate ^{10}Be data reported in previous publications using a chi-square inversion analysis of depth profiles and an updated scaling model for spatial production rate variations. We also discuss sampling strategies for dating alluvial fans in arid settings.

This study confirms the low horizontal and vertical slip rates within the massifs of the Gurvan Bogd mountain range for the Late Pleistocene–Holocene period, suggests that episodes of aggradation occurred near the times of major global glacial terminations (at ca. 15–20 ka and ca. 100–130 ka), and provides evidence for another much earlier aggradational episode, occurring before 400 ka. The Bogd fault has a maximum horizontal left-lateral slip rate of ~1.5 mm/yr, while reverse fault segments along the Gurvan Bogd fault system have vertical slip rates between 0.1 and 0.2 mm/yr. Characteristic dislocations observed along the Bogd fault suggest return periods of earthquakes similar to 1957 between 3000 and 4000 yr.

Keywords: Mongolia, Gurvan Bogd, active faults, slip rates, ^{10}Be.

†E-mail: ritz@dstu.univ-montp2.fr.

Ritz, J.-F., Vassallo, R., Braucher, R., Brown, E.T., Carretier, S., and Bourlès, D.L., 2006, Using in situ–produced ^{10}Be to quantify active tectonics in the Gurvan Bogd mountain range (Gobi-Altay, Mongolia), *in* Siame, L.L., Bourlès, D.L., and Brown, E.T., eds., Application of cosmogenic nuclides to the study of Earth surface processes: The practice and the potential: Geological Society of America Special Paper 415, p. 87–110, doi: 10.1130/2006.2415(06).

INTRODUCTION

In intraplate domains, strain rates can be very low, and earthquake recurrence intervals may be thousands of years. It is therefore important to study active faulting over several seismic cycles. In such regions, long-term slip rates determined through dating surficial features that accumulated deformation over significant timescales provide a means of characterizing tectonic activity. However, until the mid-1990s, dating morphological features displaced along active faults was problematic. In arid domains, for example, the absence of organic material and fine-grained deposits often precluded radiocarbon or thermoluminescence dating, so ages of morphological markers were typically estimated by correlation with global and regional climatic events. The development of cosmic-ray exposure dating in the mid-1980s (Nishiizumi et al., 1986; Klein et al., 1986) provided the possibility to determine surface exposure age of quartz-rich detrital material.

In this paper, we present an updated synthesis of a series of morphotectonic studies (Ritz et al., 1995, 2003; Carretier, 2000; Carretier et al., 2002; Vassallo et al., 2005) that aimed to determine the long-term slip rates along the Gurvan Bogd fault system in the Gobi-Altay (Mongolia) using in situ–produced ^{10}Be (Fig. 1). These studies were based on five months of fieldwork during seven expeditions. The Gurvan Bogd fault system is within the easternmost extent of the Mongolian Gobi-Altay, and in 1957 was the site of one of the strongest intraplate earthquakes of the past century (Mw 8.1; Florensov and Solonenko, 1965; Kurushin et al., 1997). This earthquake generated more than 350 km of surface ruptures, principally along the east-west-trending left-lateral Bogd strike-slip fault. The Bogd fault was the site of one of the first studies (Ritz et al., 1995)—along with a site along the Owens Valley fault in California (Bierman et al., 1995)—that applied cosmic-ray exposure dates to estimate long-term slip rates. Because of the arid climate, the Gobi-Altay offers extraordinary preservation of the morphological markers and thus is well suited for cosmogenic dating.

The ^{10}Be studies in Gobi-Altay, as well as others in similar settings (e.g., Anderson et al., 1996; Repka et al., 1997; Van der Woerd et al., 1998, 2002; Hancock et al., 1999; Brown et al., 2002; Meriaux et al., 2004, 2005), showed that superficial samples often contain inherited ^{10}Be due to preexposure that can lead to overestimation of their exposure ages. Measurement of the distribution of ^{10}Be with depth and comparison with theoretically predicted exponential decreases in vertical profiles (e.g., Brown et al., 1992) provide a means of evaluating complex exposure histories. Therefore, after a first protocol consisting of sampling only the surface, a second protocol consisted of analyzing the distribution of ^{10}Be at depth along soil pits dug into the upper two meters of studied markers. Below this depth and for deposits younger than a few 100 ka, negligible ^{10}Be is produced. Assuming that there was little temporal variability in the inherited component, the concentration profiles tend toward an asymptotic value at depth that indicates average inheritance, and may be used to correct the surface age (Burbank and Anderson, 2001, p. 50–51).

The distribution of ^{10}Be at depth is also a function of the erosion rate of the surface (Brown et al., 1995). Therefore, the knowledge of this parameter improves the precision of age calculations. When the erosion rate cannot be estimated, an assumption of no erosion is generally made to obtain minimum exposure ages (e.g., Brown et al., 1992; Ritz et al., 1995). The divergence between minimum and real exposure ages increases with the age of the surface, especially for surfaces older than ca. 100 ka. Indeed, the evolution of the ^{10}Be concentration of a sample with time, at a given depth and for a given production rate, firstly increases linearly and then tends to a steady-state equilibrium, which is reached more or less rapidly depending on the erosion rate (Brown et al., 1991). Using a novel chi-square inversion analysis of depth profiles (Siame et al., 2004), we reevaluate the cosmic-ray exposure data obtained for the Gurvan Bogd fault system in eastern Gobi-Altay reported in previous publications (Ritz et al., 1995, 2003; Carretier, 2000; Vassallo et al., 2005). We applied to all of them the same scaling model for spatial production rate variation calculations (Stone, 2000). This allows a discussion of contributions of morphological and tectonic processes in active fault systems.

TECTONIC SETTING

The Gobi-Altay mountain range in Mongolia and its continuation to the northwest, the Altay mountain range, represent the northernmost active compressional belt in central Asia (Molnar and Tapponnier, 1975; Tapponnier and Molnar, 1979) (Fig. 1). Western Mongolia and its immediately surrounding areas were the site of four M 8 earthquakes during the twentieth century, and thus may be considered among the most active intracontinental regions (e.g., Baljinnyam et al., 1993; Schlupp, 1996; Bayasgalan, 1999).

In 1957 the most recent of these earthquakes, the Gobi-Altay earthquake, ruptured the eastern part of the Valley-of-Lakes fault (called the Bogd fault), a Paleozoic structure that was reactivated during the Cenozoic (Florensov and Solonenko, 1965). The following year, a Mongolian-Russian expedition provided an outstanding description of ground surface effects of the earthquake at the epicentral zone (Florensov and Solonenko, 1965). Baljinnyam et al. (1993) revisited some of the piercing points of the surface breaks, and Kurushin et al. (1997) furnished an updated and thorough description of the entire rupture area. The main rupture of more than 260 km of left-lateral strike slip occurred along the Bogd fault, to the north of the Ih Bogd (3957 m) and Baga Bogd (3590 m) massifs (Fig. 1). The average horizontal displacement ranged between 3 and 4 m with a maximum section of offsets up to 5–7 m (Kurushin et al., 1997). An additional 100 km of reverse faulting, distributed on five secondary segments, ruptured simultaneously with the Bogd fault during the 1957 earthquake (Ölziyt, Gurvan Bulag, Toromhon, Dalan Türüü, and Hetsüü). These fault segments correspond mainly to thrust faults found at the base of ridges and low hills or "forebergs" (Florensov and Solonenko, 1965; Kurushin et al., 1997; Owen et al., 1999; Bayasgalan et al., 1999b) that are shortening structures associated with the main Bogd strike-slip fault.

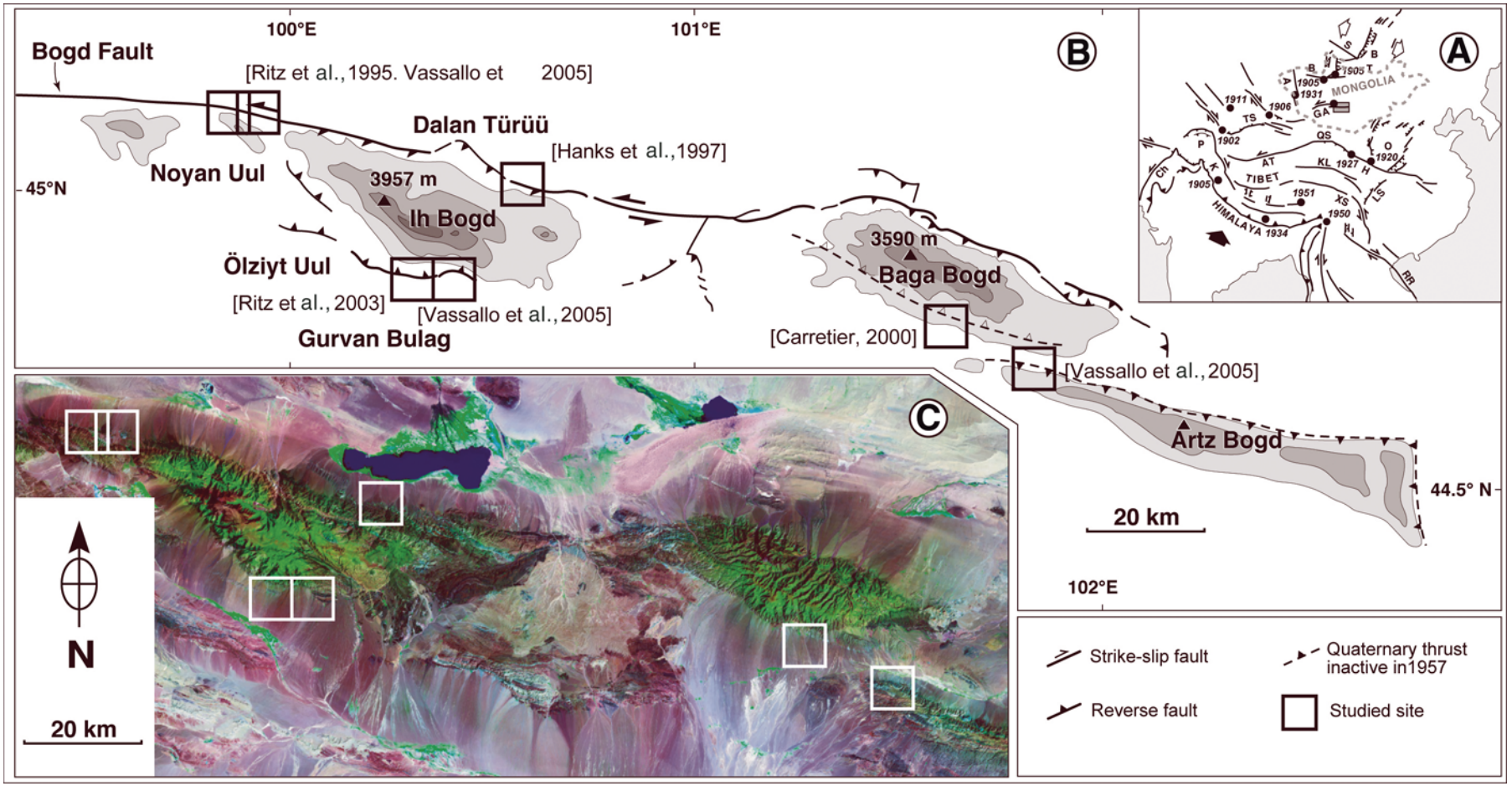

Figure 1. A: Simplified map of Quaternary faults in central Asia and M ≥ 8 earthquakes (solid dots) recorded during the past century (modified after Molnar and Qidong, 1984). B—Baikal; S—Sayan; T—Tsetserleg; B—Bolnay; A—Altay; GA—Gobi-Altay; TS—Tien Shan; P—Pamir; AT—Altyn Tagh; QS—Qilian Shan; O—Ordos; H—Haiyuan; KL—Kunlun; LS—Lungmen Shan; XS—Xian Shui; RR—Red River; K—Karakorum; Ch—Chaman. B: Sketch map of the 1957 Gobi-Altay rupture. Dashed lines are fault ruptures that did not break in 1957. Open squares are sites where slip-rate estimations were made using in situ–produced ^{10}Be dates. A and B modified after Ritz et al., 2003. C: Landsat image showing the Gurvan Bogd mountain range and the studied sites.

The topography of the region appears to be tightly associated with the geometry, the kinematics, and the distribution of ruptures (Fig. 1). Along the Ih Bogd and Baga Bogd massifs, left-lateral slip is associated with a vertical reverse component. These two massifs are bounded by oblique reverse faults along their northern flanks and pure reverse faults along their southern flanks. They can thus be considered as rigid pop-up structures resulting from transpressional deformations within restraining bends along the Bogd strike-slip fault (Kurushin et al., 1997; Cunningham et al., 1996, 1997; Cunningham, 1998). The broad flatness of the summit plateau of the Ih Bogd massif (Fig. 2), an elevated remnant of an ancient erosional surface, also suggests that the bounding faults have had similar long-term slip rates. The difference in height between the surface and the bounding faults is ~2000 m.

Morphological analysis of offset streams, ridges, or alluvial fans along the Gurvan Bogd fault system permits estimation of cumulative displacements. This allows evaluation of the late Quaternary slip rates along the various fault segments involved in building the mountain range. Vertical slip rates along the reverse faults allow estimation of the time since initiation of relief uplift, while the horizontal slip rate combined with analysis of coseismic displacements along the Bogd strike-slip fault allows calculation of the recurrence interval of large earthquakes in the area.

FIELDWORK AND METHODS

Field Site Selection

Soviet-Mongolian aerial photographs (1:35,000 scale) taken in 1958 were used to define surfaces and to choose sites for detailed field studies, selecting those with the best-preserved morphotectonic markers (typically fan surfaces displaced by fault movements [Fig. 3] and their associated surface features, mainly debris flows). Based on their general appearance, the studied morphotectonic markers can be categorized into groups with qualitatively decreasing age. The oldest markers are rounded ridges corresponding to remnants of alluvial surfaces that have been reincised by the drainage network. Boulders on such features are entirely embedded in the surface. Inset in these ridges, two to three flat surfaces are recognizable: The older, flatter surfaces contain deeply weathered granite boulders generally embedded in finer material (debris flows); the younger surfaces are broader and can be covered by broad debris-flow deposits characterized by dense boulder fields (according to the lithology of the bedrock within the upstream drainage basin). The well-preserved granite boulders (1 m on average, up to 3 m) on the different surfaces often show well-developed desert varnish coatings, some of which having petroglyphs reported to be 3000 yr old (Florensov and Solonenko, 1965) (Fig. 4).

Measurement of Offsets

Topography of the surfaces was surveyed by measuring cross sections or digital elevation models (DEMs) with kinematic GPS using two receivers. One was used as a base, its antenna fixed on a tripod; the other one was mobile, its antenna attached to a hand-carried pole. Both receivers recorded positioning data (from at least four satellites) at intervals of 1, 3, 5, or 10 seconds depending on the length of profiles or the surface of the DEM and the need for finer topographic details. Positioning data were processed after or during (by means of a radio connection between receivers) the survey depending on the type of kinematic GPS stations. Remeasurements of starting points for profiles or DEM indicated horizontal and vertical uncertainties on the order of 1 cm. Displacements and associated uncertainties were calculated using mathematical parameterizations developed by Hanks et al. (1984) from the work of Bucknam and Anderson (1979).

Dating Morphotectonic Markers

Cosmic-ray exposure dating of the morphological markers was performed using in situ–produced ^{10}Be (e.g., Brown et al., 1991; Bierman, 1994; Siame et al., 2000). The alluvial fans cut by the Gurvan Bogd fault system show variations in morphology and degree of preservation. Our sampling strategy was developed to minimize the effects of exposure prior to deposition and of postdeposition erosional processes. Some of the surfaces show dense boulder fields preserved at the surface, whereas some others—because they are older and more eroded or because they are composed of material with other lithologies—do not contain large boulders. Our sampling strategies evolved over time. At the beginning of the study in 1993, the working assumption was that the occurrence of large granite boulder flows represented the effect of strong erosional events that reworked massive quantities of slope material from the upstream drainage basins (Ritz et al., 1995, 2003). In addition, because these debris flows represented intense erosional events, it was thought that deposition would be rapid, and little cosmogenic nuclide accumulation would occur during transport. Under these conditions, the concentration of in situ cosmogenic ^{10}Be would be directly related to the time when alluviation ended, or when subsequent incision led to the abandonment of the fan surface.

However, during evaluation of first ages obtained from surface samples (Ritz et al., 1995), we realized that some of these surface boulders were likely to contain ^{10}Be due to prior exposure. This inherited ^{10}Be leads to the overestimation of exposure ages. In subsequent fieldwork, we collected samples for ^{10}Be analysis in depth profiles in fan surfaces in order to evaluate the potential role of prior exposure (Carretier, 2000; Ritz et al., 2003; Vassallo et al., 2005). Observations of the evolution of ^{10}Be with depth may be compared with theoretically predicted exponentially decreasing profiles (e.g., Brown et al., 1992, 1995) to develop strategies for corrections for prior exposure.

To estimate exposure ages from boulders embedded in alluvial fans as well as both denudation rates and exposure ages from depth profiles, the following equation was used:

Figure 2. A: SPOT image of Ih Bogd massif (note the flat summit surface covered by a thin snow cap). B: Ih Bogd massif seen from the Dalan Türüü thrust fault. C: View toward the east of Ih Bogd summit surface corresponding to an old erosional surface.

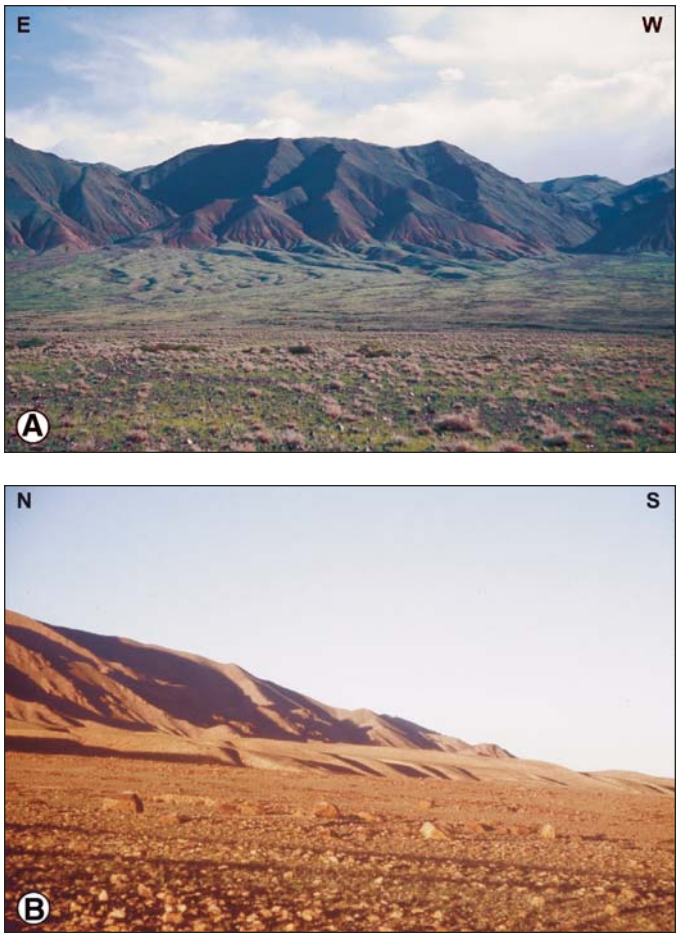

Figure 3. Examples of offset alluvial fan surfaces. A: Along the Bogd left-lateral strike-slip fault. B: Along the Gurvan Bulag thrust fault at Noyan Uul.

Figure 4. Large boulder (~1 m diameter) exposed at the surface of a fan, well embedded in finer material. Note the petroglyph representing a ram drawn on the heavy desert varnish coating. Note also the absence of desert varnish at the bottom of the boulder, attesting to the erosion of the finer material by wind deflation.

$$C(x,\varepsilon,t) = C_{inh}\cdot e^{-\lambda t} + \frac{P_0\cdot p_n}{\frac{\varepsilon}{\Lambda_n}+\lambda}\cdot e^{-\frac{x}{\Lambda_n}}\left[1-e^{-t\left(\frac{\varepsilon}{\Lambda_n}+\lambda\right)}\right] + \frac{P_0\cdot p_{us}}{\frac{\varepsilon}{\Lambda_{us}}+\lambda}$$

$$\cdot e^{-\frac{x}{\Lambda_{us}}}\left[1-e^{-t\left(\frac{\varepsilon}{\Lambda_{us}}+\lambda\right)}\right] + \frac{P_0\cdot p_{uf}}{\frac{\varepsilon}{\Lambda_{uf}}+\lambda}\cdot e^{-\frac{x}{\Lambda_{uf}}}\left[1-e^{-t\left(\frac{\varepsilon}{\Lambda_{uf}}+\lambda\right)}\right] \quad (1)$$

where $C(x, \varepsilon, t)$ is the ^{10}Be concentration function of depth x (g/cm^2), erosion rate ε (g/cm^2/yr) and exposure time t (yr); Λ_n, $\Lambda_{\mu s}$, and $\Lambda_{\mu f}$ are the effective apparent attenuation lengths (g/cm^2), for neutrons, slow muons, and fast muons, respectively; p_n, $p_{\mu s}$, and $p_{\mu f}$ are the relative contributions to the ^{10}Be production rate of the three reactions ($p_n + p_{\mu s} + p_{\mu f} = 100\%$); P_0 is the production rate at the surface taken from Stone (2000); and C_{inh} represents the ^{10}Be concentration potentially acquired by the sample during exposure to cosmic rays prior to emplacement in their sampling position. All calculations were performed using attenuation lengths of 150, 1500, and 5300 g/cm^2 with associated relative contributions to the total surface production rate of 97.85%, 1.50%, and 0.65% for neutrons, slow muons and fast muons, respectively. These values are based on field-calibrated measurements (Braucher et al., 2003).

Recently, Siame et al. (2004) showed that measurement of ^{10}Be concentrations along a depth profile allows estimation of both exposure time and erosion rate using a chi-square inversion that minimizes the function

$$Chi-square = \sum_{i=1}^{n}\left[\frac{C_i - C_{(x_i,\varepsilon,t)}}{\sigma_i}\right]^2, \quad (2)$$

where C_i is the measured ^{10}Be concentration at depth x_i, $C(x_i, \varepsilon, t)$ is the theoretical ^{10}Be concentration determined using equation 1, σ_i is the analytical uncertainty at depth i, and n is the total number of samples in the profile. Chi-square inversion allows us to determine the Q value, an estimator of the "goodness of fit" (e.g., Press et al., 1996). The model is considered a good one if the Q value is greater than 0.001. A lower value can result from oversimplifying model assumptions (such as constant erosion rate through time or same inheritance for all samples), or from too large analytical uncertainties.

For each profile, we assume a null inheritance and an inheritance of 0.15 M atoms/g to evaluate the effects of inheritance on age determination. The second value corresponds to the typical concentration measured in samples at depths greater than 1.5 m. This concentration would correspond to a residence time of 5000 yr at the average elevation of the major drainage basins feeding the alluvial fans. For both values, we generated a chi-square contour diagram versus erosion rate and time. The minimum chi-square value defines the best-fit erosion-time couple. A 1σ confidence interval contour is determined, whose projection

on erosion and time axes determines 1σ uncertainties associated with the best-fit couple. However, these chi-square contour diagrams usually display a vertical trend parallel to the time axis for large ages. If the best-fit solution lies in this portion of the diagram, the best-fit model corresponds to a steady state, for which the determination of the age is impossible. In this case, calculation only yields an erosion rate and a minimum age, which corresponds to the minimum chi-square value for no erosion.

For the surficial samples of each studied surface, a mean exposure age, weighted to account for the variable analytical uncertainties for each sample, was computed. To perform this calculation, we did not include outlying data that were significantly different (when considering 2σ uncertainty intervals) from the mean value of the main data cluster for a given feature. Such outliers are interpreted as being associated either with reworked material with significant predepositional exposure (highest values), or with material exposed to postdepositional processes (lowest values). The uncertainty for the age of each surface was then estimated by the difference between this weighted mean age and the highest and lowest considered ages (error bars included), since we do not know whether scatter is primarily due to variation in inheritance (predepositional exposure) or erosion/shielding (postdepositional processes). Because the erosion rate affecting surficial boulders may be significantly different (lower) than the erosion rate estimated for the corresponding surfaces, the exposure ages of boulders were calculated assuming no erosion and are therefore minimum ages. These minimum ages allow us to check the validity of the ages obtained from the depth profiles. We use preferably ages obtained from the depth profiles because they give more accurate ages. The ages obtained from surficial samples are used only if ages given by depth profiles are poorly constrained.

Samples were analyzed by accelerator mass spectrometer at the Tandétron AMS facility, Gif-sur-Yvette, France (Raisbeck et al., 1987, 1994) or the Lawrence Livermore National Laboratory AMS facility, Livermore, California, USA (Davis et al., 1990), after isolation of quartz and chemical preparation of Be targets (Ritz et al., 2003). One goal of this paper is to homogenize and synthesize all data gathered in the region, having the ^{10}Be concentrations all normalized with reference to National Institute of Standards and Technology Standard Reference materials (NIST SRM) 4325 using its certified ^{10}Be/^{9}Be ratio of (26.8 ± 1.4) × 10^{-12} (Tables 1–4). All exposure age calculations use production rates from Stone (2000).

TABLE 1. RESULTS OF THE ^{10}Be ANALYSIS WITH ^{10}Be CONCENTRATIONS CALIBRATED DIRECTLY AGAINSTTHE NIST STANDARD REFERENCE MATERIAL SRM 4325

Sample	Surface	P0 (at/g/yr)	10Be (Mat/g)	Uncertainty (Mat/g)	Minimum age (yr)	Uncertainty (yr)
Noyan Uul						
D VI 1	S1	21.1	1.42	0.11	6.99E+04	6.85E+03
D VI 3	S1	21.1	1.30	0.17	6.39E+04	9.19E+03
D VI 4	S1	21.1	1.04	0.11	5.09E+04	6.19E+03
D VI 5	S1	21.1	1.37	0.14	6.74E+04	7.98E+03
D VII 1	S2	21.1	1.10	0.14	5.39E+04	7.59E+03
D VII 2	S2	21.1	1.56	0.17	7.69E+04	9.56E+03
D VII 3	S2	21.1	1.83	0.12	9.05E+04	8.04E+03
D VII 4	S2	21.1	1.65	0.14	8.14E+04	8.46E+03
D VII 5	S2	21.1	1.55	0.12	7.6E+04	7.48E+03
D IV 1	R1	21.1	1.30	0.09	6.39E+04	5.85E+03
D IV 2	R1	21.1	1.13	0.08	5.54E+04	5.14E+03
D IV 3	R1	21.1	1.22	0.10	5.99E+04	6.08E+03
D IV 4	R1	21.1	0.97	0.09	4.75E+04	5.25E+03

Soil pit	Surface	Depth (cm)	10Be (Mat/g)	Uncertainty (Mat/g)
NU42	S1	205	0.34	0.06
NU45	S1	160	0.63	0.14
NU47	S1	110	0.45	0.07
NU49	S1	80	0.32	0.04
NU51	S1	20	1.11	0.16
NU52A	S1	0	1.85	0.27

P0 (at/g/yr)	Density (g/cm^3)
18.2	2.0

Note: Uses its certified ^{10}Be/^{9}Be ratio of (26.8 ± 1.4) × 10^{-12} and cosmic ray exposure ages at Noyan Uul.

TABLE 2A. CENTRAL GURVAN BULAG, WESTERN FAN

Sample	Surface	P0 (at/g/yr)	10Be (Mat/g)	Uncertainty (Mat/g)	Minimum age (ka)	Uncertainty (ka)
Gurvan Bulag (West)						
GB96-9	S2	25.0	3.05	0.10	1.29E+05	8.85E+03
GB96-10	S2	25.0	3.19	0.10	1.35E+05	9.12E+03
GB96-11	S2	25.0	3.17	0.08	1.34E+05	8.67E+03
GB96-12	S2	25.0	2.99	0.07	1.26E+05	8.15E+03
GB96-13 (65 cm)	S2	25.0	1.18	0.03		
GB96-14 (90 cm)	S2	25.0	0.84	0.03		
GB96-13†	S2	25.0	2.81	0.31	1.18E+05	1.47E+04
GB96-14†	S2	25.0	2.79	0.32	1.17E+05	1.50E+04
GB96-15‡	S2	25.0	2.10	0.05	8.77E+04	5.66E+03
Mo93-AII1	S3	25.0	0.28	0.03	1.17E+04	1.42E+03
Mo93-AII2	S3	25.0	0.29	0.04	1.21E+04	1.79E+03
Mo93-AII3	S3	25.0	0.43	0.04	1.75E+04	1.95E+03
Mo93-AII4	S3	25.0	0.59	0.05	2.44E+04	2.52E+03
Mo93-AII5‡	S3	25.0	1.02	0.08	4.22E+04	4.16E+03
Mo95-11	S3	25.0	0.37	0.03	1.53E+04	1.54E+03
Mo95-12	S3	25.0	0.29	0.02	1.20E+04	1.09E+03
Mo95-13	S3	25.0	0.32	0.02	1.32E+04	1.14E+03
Mo95-14	S3	25.0	0.42	0.05	1.73E+04	2.30E+03
Mo95-15	S3	25.0	0.44	0.03	1.82E+04	1.62E+03
Mo95-16	S4	24.1	0.11	0.01	4.50E+03	5.03E+02
Mo95-17	S4	24.1	0.21	0.03	8.75E+03	1.22E+03
Mo95-18	S4	24.1	0.08	0.01	3.37E+03	5.88E+02
Mo95-19	S4	24.1	0.13	0.02	5.43E+03	7.92E+02
Mo95-20‡	S4	24.1	0.36	0.03	1.54E+04	1.52E+03
Mo95-21‡	S5	24.1	1.39	0.08	5.98E+04	4.84E+03
Mo95-22	S5	24.1	0.43	0.03	1.83E+04	1.83E+03
Mo95-23	S5	24.1	0.31	0.03	1.30E+04	1.42E+03
Mo95-24	S5	24.1	0.41	0.04	1.74E+04	1.88E+03
Mo95-25	S5	24.1	0.35	0.04	1.51E+04	1.83E+03

Soil pit	Surface	Depth (cm)	10Be (Mat/g)	Uncertainty (Mat/g)
GB96-1	S2	40–45	1.21	0.09
GB96-2	S2	55–60	0.89	0.06
GB96-3	S2	90	0.78	0.05
GB96-4	S2	110–115	0.50	0.04
GB96-5	S2	130	0.51	0.04
GB96-6	S2	145–148	0.44	0.04
GB96-7A	S2	160	0.25	0.09
GB96-7B	S2	160	0.21	0.02
GB96-8A	S2	170	0.18	0.02
GB96-8B	S2	172	0.19	0.03

P0 (at/g/yr)	Density (g/cm^3)
25.0	2.0

†Data normalized to the surface.
‡Outlying data not included in calculations (see text).

TABLE 2B. CENTRAL GURVAN BULAG, EASTERN FAN

Soil pits	Surface	Depth (cm)	^{10}Be (Mat/g)	Uncertainty (Mat/g)
Gurvan Bulag (East)				
IBSA23	S2	140	0.54	0.07
IBSA25	S2	100	0.73	0.09
IBSA26	S2	70	1.37	0.19
IBSA28	S2	30	1.79	0.20
IBSA30	S2	0	2.54	0.27
IBSB31	S3	200	0.16	0.04
IBSB33	S3	160	0.38	0.05
IBSB35	S3	120	0.15	0.03
IBSB37	S3	80	0.37	0.05
IBSB39	S3	40	0.50	0.07
IBSB41	S3	0	0.70	0.10

P0 (at/g/yr)	Density (g/cm^3)
23.3	2.0

TABLE 3. SOUTH BAGA BOGD

Sample	Surface	P0 (at/g/yr)	^{10}Be (Mat/g)	Uncertainty (Mat/g)	Minimum age (yr)	Uncertainty (yr)
South Baga Bogd						
BBS97-1†	S3	27.6	1.68	0.04	6.47E+04	4.20E+03
BBS97-2	S3	27.6	0.52	0.05	1.85E+04	2.02E+03
BBS97-3	S3	27.6	0.63	0.02	2.23E+04	1.57E+03
BBS97-4	S3	27.6	0.53	0.05	1.86E+04	2.03E+03
BBS97-5†	S3	27.6	1.40	0.03	5.26E+04	3.38E+03

Soil pit	Surface	Depth (cm)	10Be (Mat/g)	Uncertainty (Mat/g)
BBS97-18	S1	0	2.85	0.11
BBS97-15	S1	60	1.61	0.01
BBS97-12	S1	110	0.99	0.11
BBS97-11	S1	130	0.94	0.12
BBS97-9	S1	160	0.39	0.09
BBS97-8	S1	185	0.56	0.04
BBS97-6	S1	220	0.22	0.03

P0 (at/g/yr)	Density (g/cm^3)
27.6	2.0

†Outlying data not included in calculations (see text).

SUMMARY OF PREVIOUS RESULTS

The Bogd Fault: Noyan Uul

At Noyan Uul, immediately to the northwest of the Ih Bogd massif (location in Fig. 1), there are morphological features clearly displaying cumulative horizontal left-lateral displacements (Fig. 5). The east-southeast-trending fault scarp delimits two morphological domains: (1) to the south a mountainous area incised by gorges and deep ravines and (2) to the north an alluvial plain that dips gently (5°) northward. The drainage network clearly shows small-scale left-lateral strike-slip movements; along the fault an ~5 m offset is visible, and numerous small streams show left-lateral displacements. North of the fault scarp there are several generations of incised alluvial fans. The younger fans (S0) are cone-shaped in plan view. During deposition, they truncated parts of the older fans. The old fans (S1, S2) do not presently correspond to any upslope stream, indicating sinistral displacement of the alluvial plain relative to the mountainous domain. Ritz et al. (1995) studied the site where the misalignment of cones with respect to the drainage basin was clearest and where the left-lateral strike-slip offset was also manifested by the misalignment of large stream incisions in the old alluvial fans (D1, D2), which appear beheaded relative to streams upslope of the fault (Fig. 6). Simultaneous alignment of floodplain features (S2, D1, and D2) with upslope streams (U0, U1, and U2, respectively) requires compensation for a 220 ± 10 m horizontal offset, while alignment of surface S1 apex with the outlet of the upstream drainage basin requires compensation for 110 ± 10 m. The incision of valleys U1-D1 and U2-D2 in the hanging wall and the deposition of alluvial fans S0, S1, and S2 in the footwall can be interpreted as the result of enhanced stream power associated with a major regional climate change (Carretier et al., 1998).

TABLE 4. NORTH ARTZ BOGD

Soil pit	Surface	Depth (cm)	^{10}Be (Mat/g)	Uncertainty (Mat/g)
North Artz Bogd				
ABW1	UNIT 1	200	0.42	0.10
ABW4	UNIT 1	160	0.74	0.09
ABW6	UNIT 1	120	1.23	0.14
ABW8	UNIT 1	80	2.41	0.32
ABW10	UNIT 2	40	3.29	0.41
ABW12B	UNIT 2	0	3.39	0.37

P0 (at/g/yr)	Density (g/cm^3)
21.0	2.0

Analogously displaced fans are observed for several kilometers in both directions along the fault (Ritz, 2003).

Ritz et al. (1995) sampled S1 and S2 as well as old ridges (R1) that were interpreted as remnants of even older fan surfaces (Fig. 6). If we consider a constant slip rate through time, surface S2 should be twice as old as S1, and its boulders should have correspondingly higher ^{10}Be concentrations. Instead, Ritz et al. (1995) found that there were only small differences in ^{10}Be concentrations between the two surfaces, and that ^{10}Be concentrations of ridgetop boulders were lower than those associated with the stratigraphically younger surfaces. This suggested that the concentrations were approaching steady-state values on surfaces

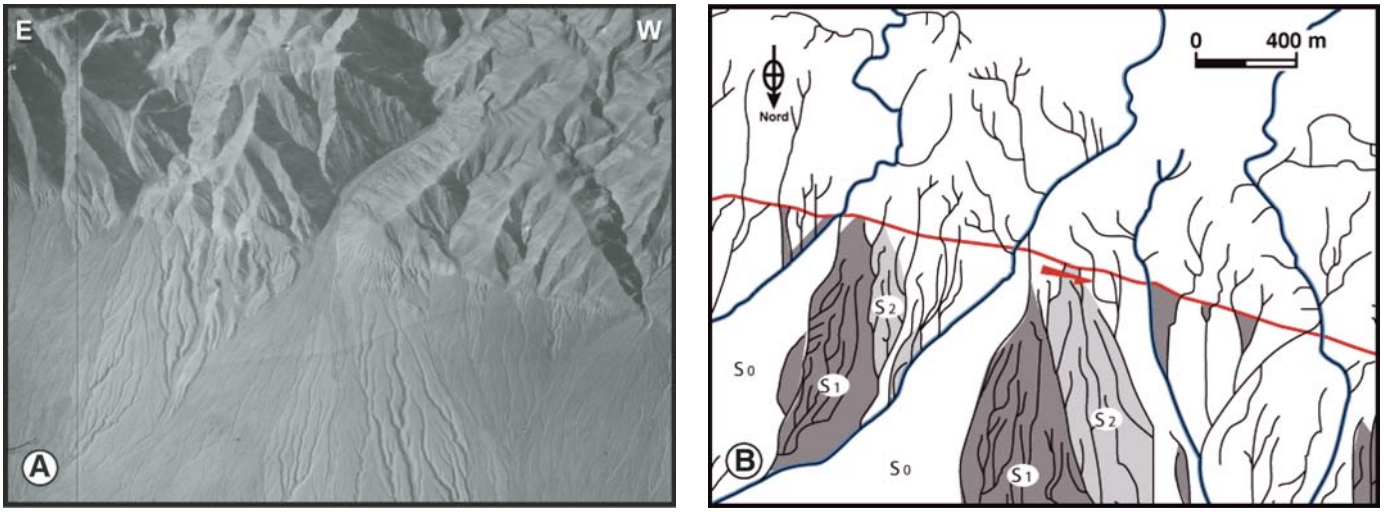

Figure 5. A and B: Aerial image and corresponding sketch map of two sequences of three alluvial fan surfaces (S0, S1, S2) shifted left-laterally along the Bogd strike-slip fault at Noyan Uul site. S0 (white) is the younger alluvial surface, S2 (light gray) is the older and S1 (dark gray) is the intermediate one. Main streams are underlined in blue.

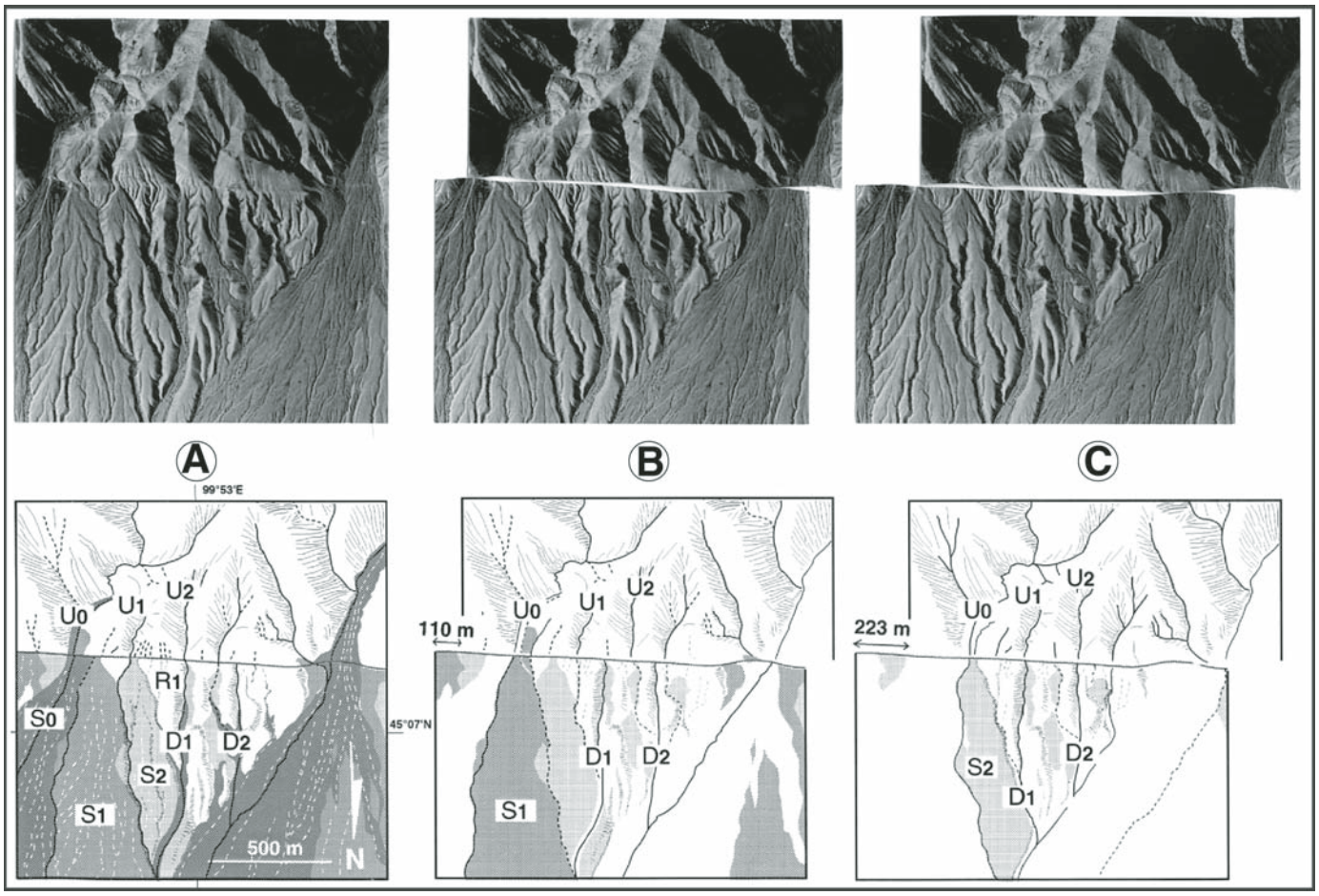

Figure 6. Reconstruction of history of alluvial fan deposition and erosion along the Bogd fault at Noyan Uul based on aerial photographs. A: Present day. B: Compensation for ~110 m horizontal offset. C: Offset compensation of ~220 m. Solid lines labeled U0, U1, and U2 designate major stream axes upstream of fault; D1 and D2 are major axes below the fault. Dotted lines indicate smaller river valleys. Shading represents relative age of depositional surfaces (S2, S1, and S0); lightest tones corresponding to oldest surfaces. Only present-day relicts of alluvial fans S1 and S2 are represented in B and C. After Ritz et al. (1995).

S1 and S2. Taking the apparent minimum age calculated for the youngest surface S1 (80 ka), Ritz et al. (1995) calculated a maximum horizontal slip rate of 1.2 mm/yr. Vassallo et al. (2005) reestimated the age of surface S1 at 125 ± 28 ka by analyzing the ^{10}Be distribution at depth—yielding an average inheritance of 0.20 ± 0.10 M atoms/g—and by estimating the erosion rate at 7 ± 1 m/m.y. This allowed the authors to calculate a left-lateral slip rate of 0.95 ± 0.29 mm/yr.

The Gurvan Bulag Thrust Fault

The Gurvan Bulag fault is a 23 km thrust that ruptured most recently in 1957, simultaneously with the Bogd strike-slip fault during the Mw 8.1 Gobi-Altay event (e.g., Kurushin et al., 1997) (Fig. 1). "Gurvan Bulag" means "three springs" in Mongolian; the 1957 earthquake changed local hydrology and dried up the springs. The morphology of the Gurvan Bulag thrust fault zone is described as a foreberg resulting from interaction between tectonics and fan dynamics (Bayasgalan et al., 1999b; Carretier et al., 2002). Flat, active surfaces are generally directly downstream of drainage basins where erosional and depositional rates are at a maximum, whereas hills are found in areas where erosion and deposition rates are lower, typically at the lateral margins of the fans. The foreberg is thus a system of inset surfaces that show clear cumulative vertical slips.

Ritz et al. (2003) and Vassallo et al. (2005) focused on two fans—termed western and eastern fans—within the central part of the Gurvan Bulag thrust fault, where the 1957 fault displacements and the cumulative deformation appear to be the largest (Fig. 7), and where the offset surfaces were the best preserved. Four markers could be distinguished from their relative elevations and surface characteristics (see Ritz et al., 2003, for more detailed description). S1 corresponds to upper, old eroded surfaces found within the hanging wall and represents elevated remnants of planar abrasive or depositional surfaces. S2 is an intermediate alluvial surface inset in S1 and is found in large patches extending on both sides of the fault. S3 is the youngest depositional surface, extending from the apex of the cones to the Gurvan Bulag foreberg, and appears to be inset in S2. Notice that the nomenclature of the surfaces, in terms of relative ages, does not correspond to that of Noyan Uul. In the western fan, as surface S3 approaches the fault zone, it overlies S2 and then dissipates before reaching the fault scarp. This termination of S3 deposits above the fault scarp is not observed within the eastern fan, where S3 is more deeply inset within the two older surfaces and crosses the fault scarp in broad channels (Fig. 7). Additional features are present only within the western fan: S4 corresponds to gullies cut in alluvial surfaces near the fault scarp, with local cones found in the footwall in front of them. Ritz et al. (2003) interpreted these features as local debris cones that accumulated at the toe of the fault scarp simultaneously with the incision of S4 gullies into older hanging-wall alluvial surfaces.

Within the western fan, Ritz et al. (2003) estimated a minimum vertical offset for S1 of 31 ± 1 m (profile 7, Fig. 8) and a mean vertical offset for surface S2 in the studied area at 19.8 ± 1.9 m (profiles 5–7, Fig. 8). Estimation of vertical slip for surface S3 was more uncertain because within the western fan S3 terminates before reaching the fault scarp and is not found at the footwall. Because of this, Ritz et al. (2003) proposed two extreme scenarios depending on whether the cumulative offset occurred before or after S3 deposition. If most of the cumulative offset occurred before S3 deposition, the minimum vertical displacement for S3 was 6.5 ± 1.2 m, corresponding to the mean vertical displacement calculated from the gullies S4 incising surface S2 (in this scenario, the S3 debris flow covered the preexisting topography of S2 by overbank flow). In contrast, if the cumulative offset occurred after deposition of S3, the measured mean vertical separation of 17.3 ± 0.4 m would represent a maximum value for the vertical offset for S3. Finally, Ritz et al. (2003) estimated from topographic analysis that the mean 1957 vertical offset along the central part of the Gurvan Bulag thrust fault was 4.2 ± 0.3 m (profiles 1–4, Fig. 8). From the offset measurements and surface ages (131 ± 20 ka and 16 ± 20 ka for S2 and S3 surfaces, respectively), Ritz et al. (2003) determined the following vertical slip rates: 0.14 ± 0.03 mm/yr over the Late Pleistocene–Holocene and between 0.44 ± 0.11 mm/yr and 1.05 ± 0.25 mm/yr since the end of the Late Pleistocene.

Within the eastern fan, Vassallo et al. (2005) studied surfaces S2 and S3. The advantage of this site—although alluvial surfaces are not covered by boulder field as on the western adjacent fan—is that these surfaces are found in both the hanging wall and the footwall, allowing more accurate estimates of vertical offsets (profiles 8 and 9, Fig. 8). The older surface is vertically displaced by 16.0 ± 0.5 m and the younger surface by 5.0 ± 0.5 m. No estimation of the 1957 offset could be made because it was clear that within the eastern fan, the frontal part of the preexisting scarp collapsed during the 1957 event (Carretier et al., 2002, defined a gravity-controlled face). This suggests that estimates of the 1957 offset made by Ritz et al. (2003) or Kurushin et al. (1997) from topography within the western fan, 2 km farther west, are too large. Ten kilometers farther east, paleoseismological evidence indicates that the 1957 vertical offset was between 1 and 2 m, and suggests that the scarp height reported along the central part of the Gurvan Bulag thrust may represent the cumulative result of repeated fault ruptures (Prentice et al., 2002). From the offset measurements and surface ages (128 ± 13 ka and 22 ± 3 ka for S2 and S3 surfaces, respectively), Vassallo et al. (2005) determined the following vertical slip rates: 0.12 ± 0.03 mm/yr over the Late Pleistocene–Holocene and between 0.23 ± 0.05 mm/yr and 0.19 ± 0.05 mm/yr since the end of the Late Pleistocene.

The Southern Baga Bogd Thrust Fault

Similarly to the Ih Bogd massif, the southern flank of the Baga Bogd massif is bounded by a 50-km-long reverse fault that cuts through the alluvial deposits (Fig. 1). Within the eastern part of the massif, Carretier et al. (2002) identified three main geomorphic surfaces (S1, S2, and S3) (Fig. 9). These surfaces

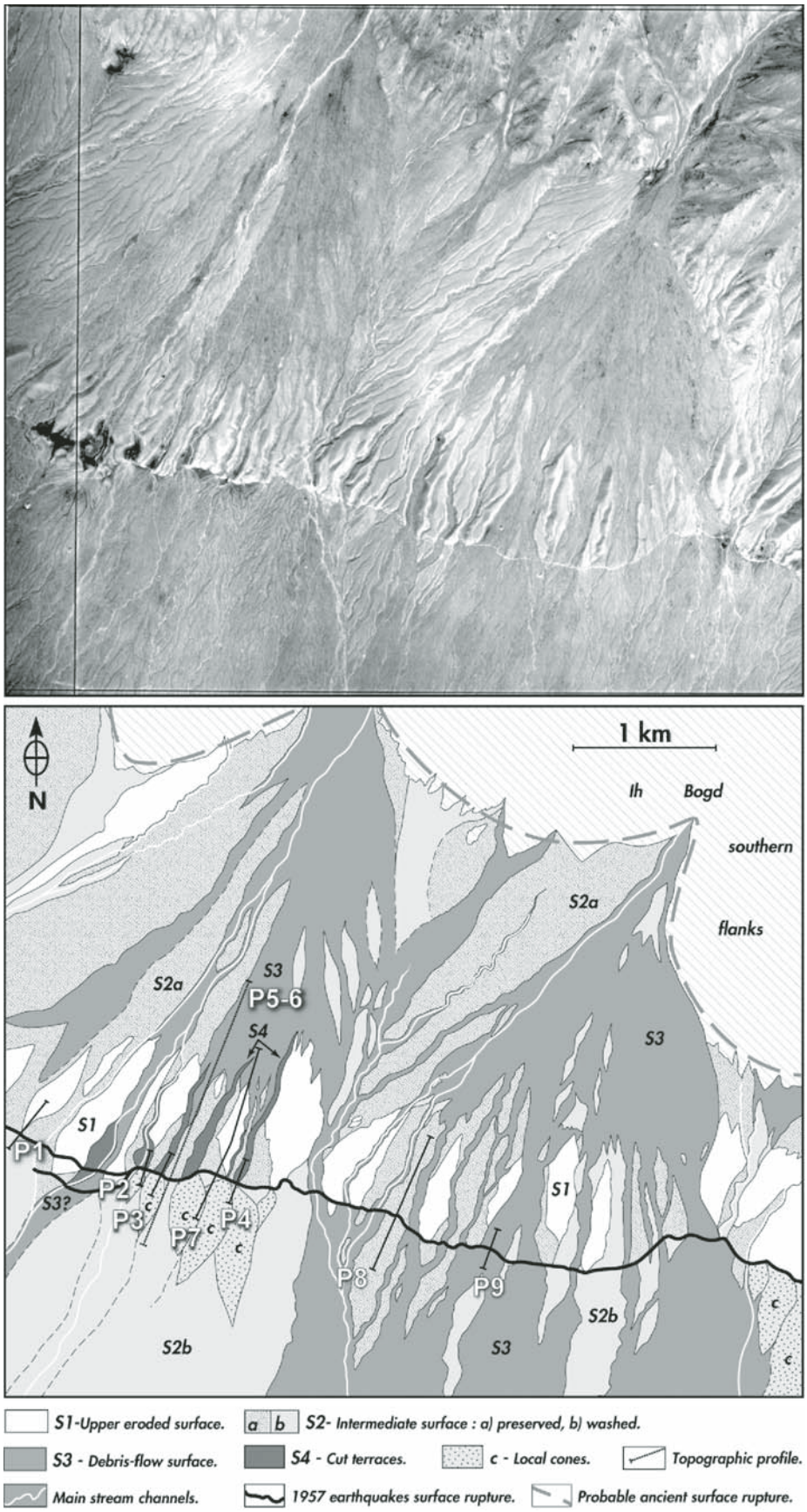

Figure 7. A: Aerial photograph of the central part of the Gurvan Bulag thrust fault cutting through two fans (see Fig. 1 for location). B: Corresponding morphological map of inset surfaces (modified after Ritz et al., 2003).

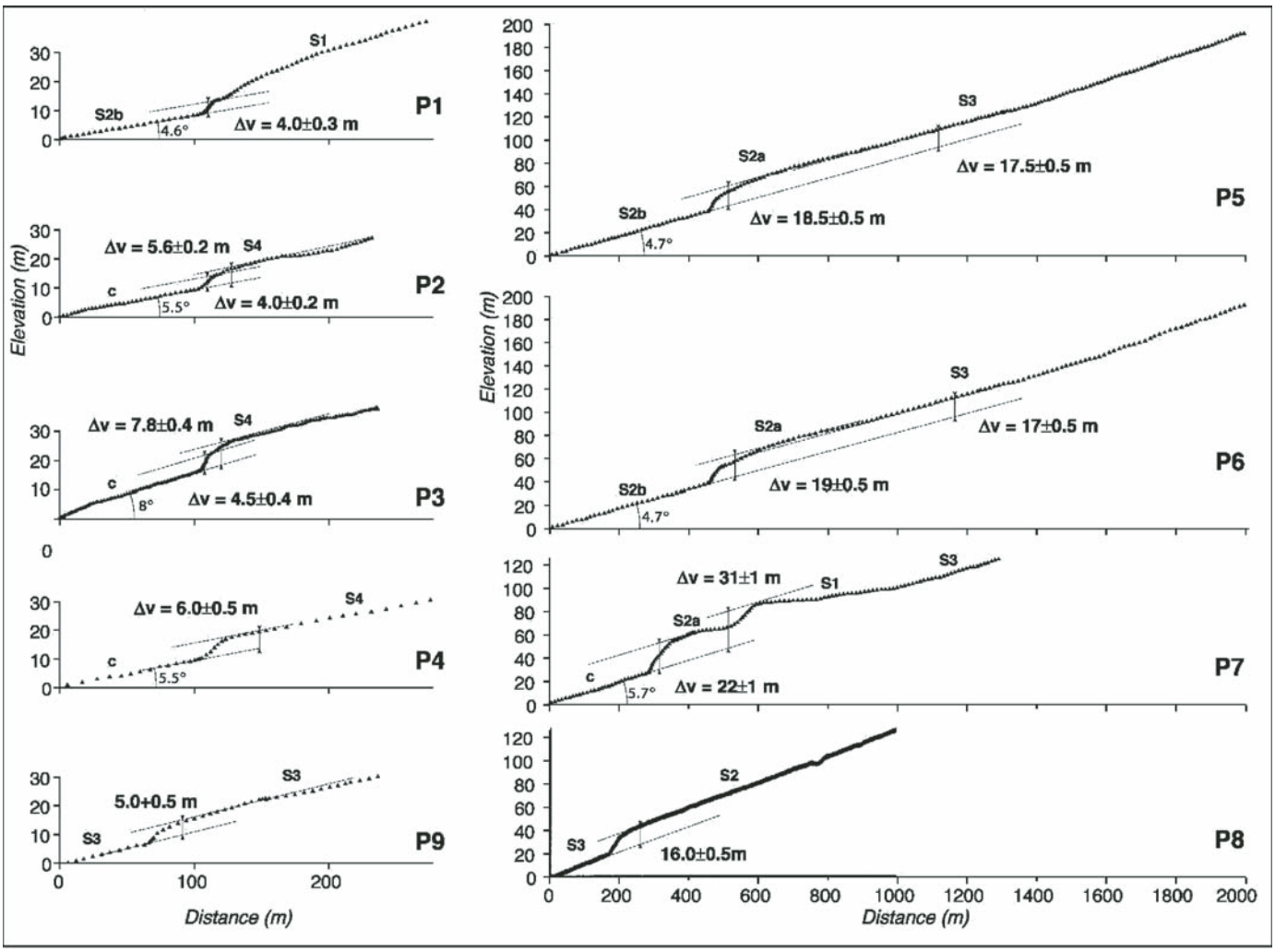

Figure 8. Topographic profiles across uplifted surfaces within the central part of the Gurvan Bulag thrust fault (see Fig. 7).

were not cut by thrusting in the 1957 earthquake (Florensov and Solonenko, 1965). The oldest (S1) is incised by dendritic drainage networks and is the highest recognizable alluvial fan surface uplifted by the reverse fault. The alluvial fan surface (S2) shows characteristics of both dendritic incision and bar-and-swales. The most recent alluvial fan surface (S3) has not been uplifted by the fault, indicating that thrust activity on this fault segment ceased between the depositions of S2 and S3. Carretier et al.'s (2002) survey of surface S1 indicated a vertical offset of 19 ± 0.5 m (Fig. 9C). They dug a soil pit in surface S1 and determined a surface age of 206 ± 50 ka, which yielded a long-term vertical slip rate of 0.10 ± 0.03 mm/yr.

The Artz Bogd Thrust Fault

The Artz Bogd thrust fault is a 75 km long fault bounding the Artz Bogd massif to the north (Fig. 1). The thrust fault is cutting through detrital slopes deposed at the piedmont of the massif (Bayasgalan et al., 1999b). Vassallo et al. (2005) studied the western termination of the fault (Fig. 10). As was the case for the western central fan studied by Ritz et al. (2003) within the Gurvan Bulag thrust fault, the surface that extends downslope of the fault scarp does not correspond to the surface that is vertically offset in the hanging wall. The hanging-wall surface was incised by the drainage network after its vertical displacement. Extension of the planar hanging-wall surface to the north indicates a vertical separation of 20.3 ± 0.5 m with respect to the footwall surface (Fig. 11A). Vassallo et al.'s (2005) analysis of the ^{10}Be concentration distribution along a soil pit dug in the hanging-wall surface shows the superposition of two depositional sequences consistently with the stratigraphy observed in the soil pit. The ages obtained for the lower and the upper layers were 360 ± 36 ka and 160 ± 16 ka, respectively. From the offset of the upper deposit (20.3 ± 0.5 m) and its exposure age, Vassallo et al. (2005) estimated a vertical slip rate of 0.13 ± 0.01 mm/yr.

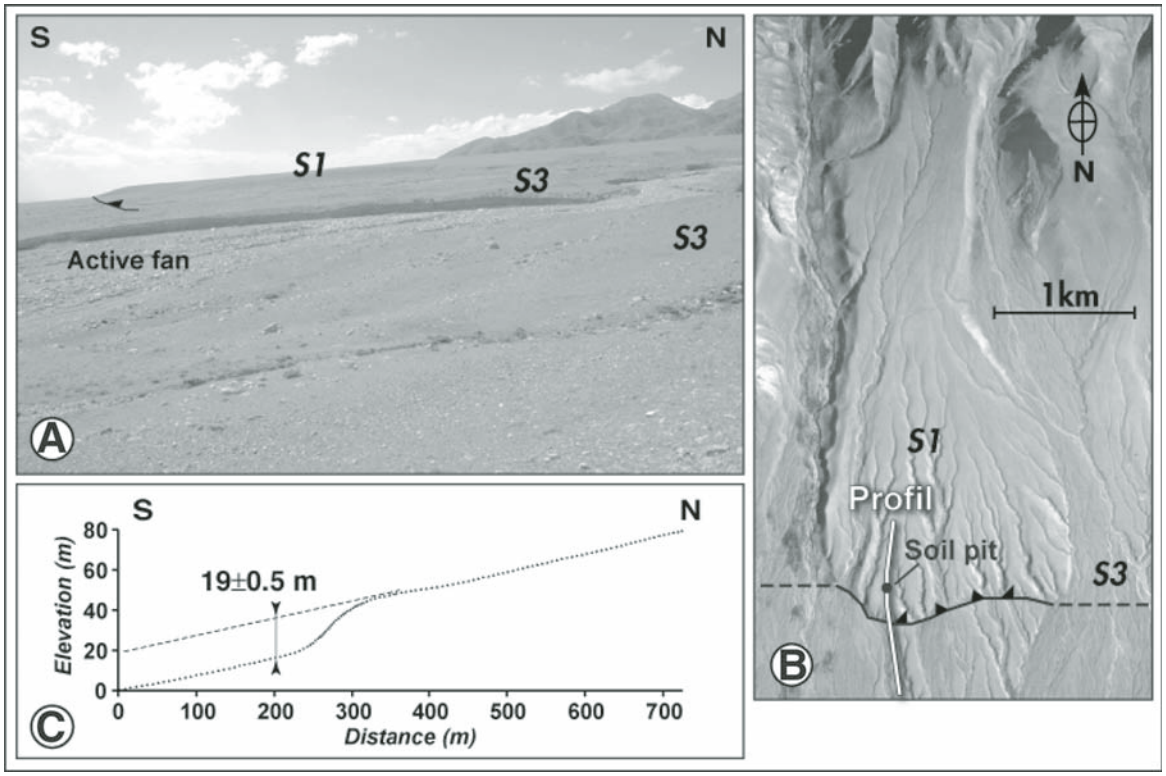

Figure 9. A: Fault scarp along the Southern Baga Bogd thrust fault. B: Corresponding site seen on aerial photograph (see Fig. 1 for location). C: Topographic profile across the fault scarp. Modified after Carretier (2000).

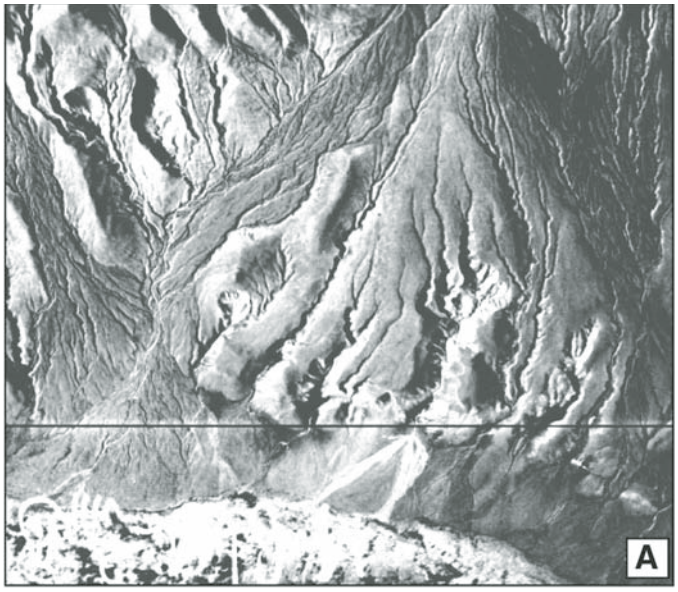

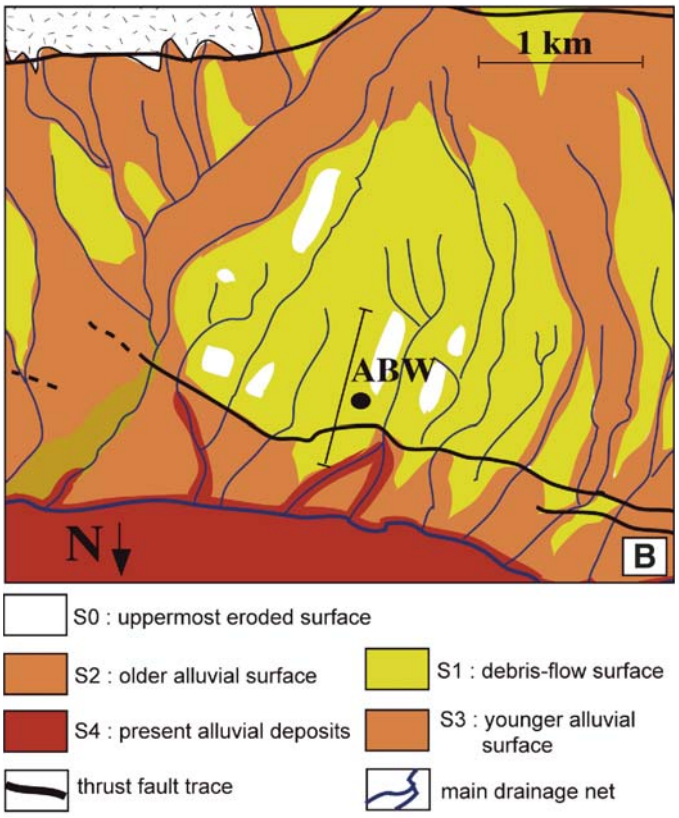

Figure 10. A: Aerial photograph of the western part of the Artz Bogd thrust fault (see Fig. 1 for location). B: Corresponding morphological map of inset surfaces. After Vassallo et al. (2005). ABW—Artz Bogd West soil pit.

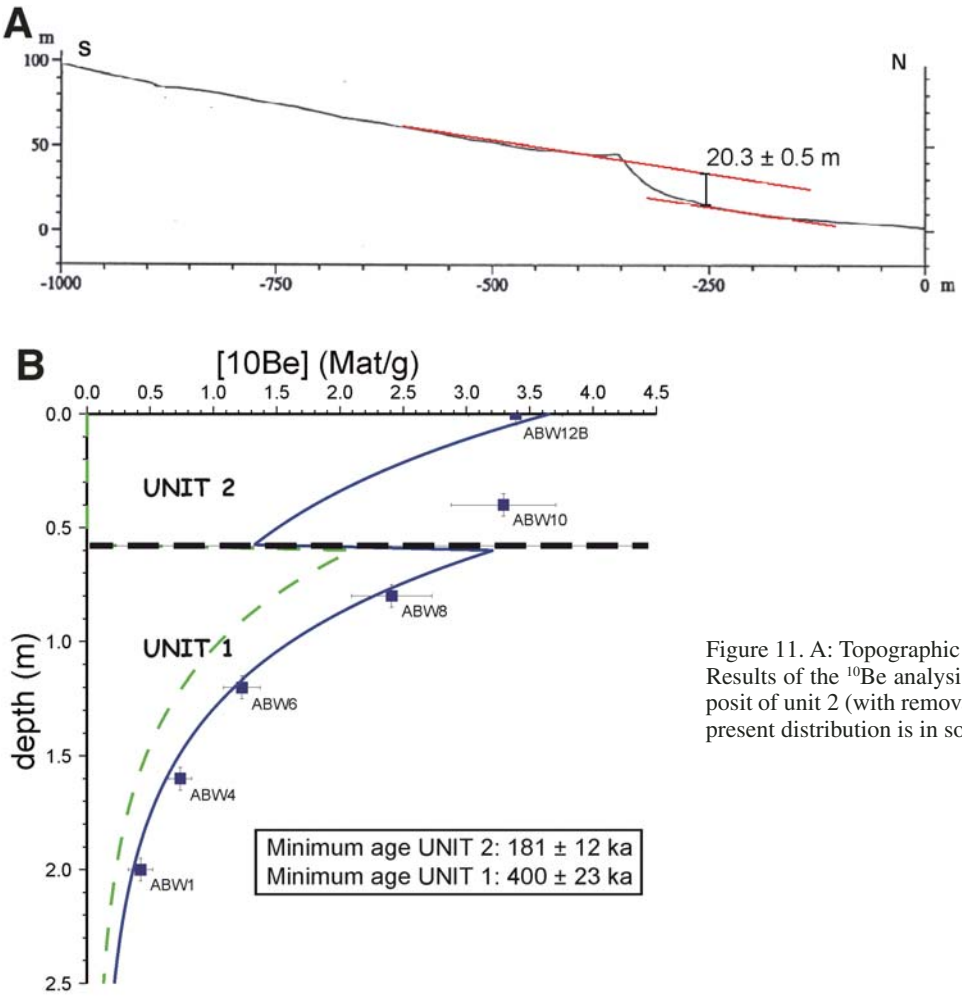

Figure 11. A: Topographic profile across the Artz Bogd fault scarp. B: Results of the ^{10}Be analysis. The ^{10}Be distribution in unit 1 before deposit of unit 2 (with removal of ~40 cm of unit 1) is in dashed line, the present distribution is in solid line. After Vassallo et al. (2005).

REEVALUATED ^{10}Be AGES

Profiles

We present results of the chi-square inversion for all the profiles in Figures 12–16 (see Tables 1–4). For the Artz Bogd site, because of the stratigraphic complexity of the deposits, we did not apply the chi-square model to the profile. However, the distribution of ^{10}Be at depth shows that there is little inherited ^{10}Be within the lower deposits (Fig. 11B). Considering no inheritance in the upper layer as well, and assuming no erosion for both units, we calculated minimum ages of 400 ± 23 ka and 181 ± 12 ka for the lower and upper depositional units, respectively.

For all profiles, except S2 in the eastern fan of Gurvan Bulag, the Q value is lower than 0.001. This is due to the scatter of samples with respect to the theoretical models, and also to the analytical uncertainties that vary significantly from one sample to another (see for instance the case of Noyan Uul, Fig. 12).

Models with the assumption of no inheritance indicate that all surfaces, except S2 at Gurvan Bulag, are at steady state. On the other hand, if we introduce an average inheritance of 0.15 M atoms/g, the models show patterns where the age of the surface is well constrained but the erosion rate for the best fit is zero, which is not realistic. Furthermore, as can be observed from the profiles or the chi-square values, the fits are not improved. Therefore, there are no mathematical reasons to prefer a model with inheritance to a model without inheritance. Nevertheless, for some surfaces (especially S3 in the eastern fan of Gurvan Bulag, the younger one) the value of the average inheritance chosen has a significant influence on the age estimation.

We found a constant optimum erosion rate value of 6 ± 1 m/m.y. for all the old surfaces, other than that at Noyan Uul. At this site, however, the scattering of samples relative to the best-fit model is large. Moreover, samples falling to the right of the best-fit curve (see Fig. 12) have greater uncertainties than other samples, diminishing their importance in the inversion process. If we do not take into account the analytical uncertainty associated with the sample at 1.6 m (lying on the right side of the model and having the largest uncertainty), the inversion leads to a best-fit erosion rate of 6 m/m.y. (Fig. 12).

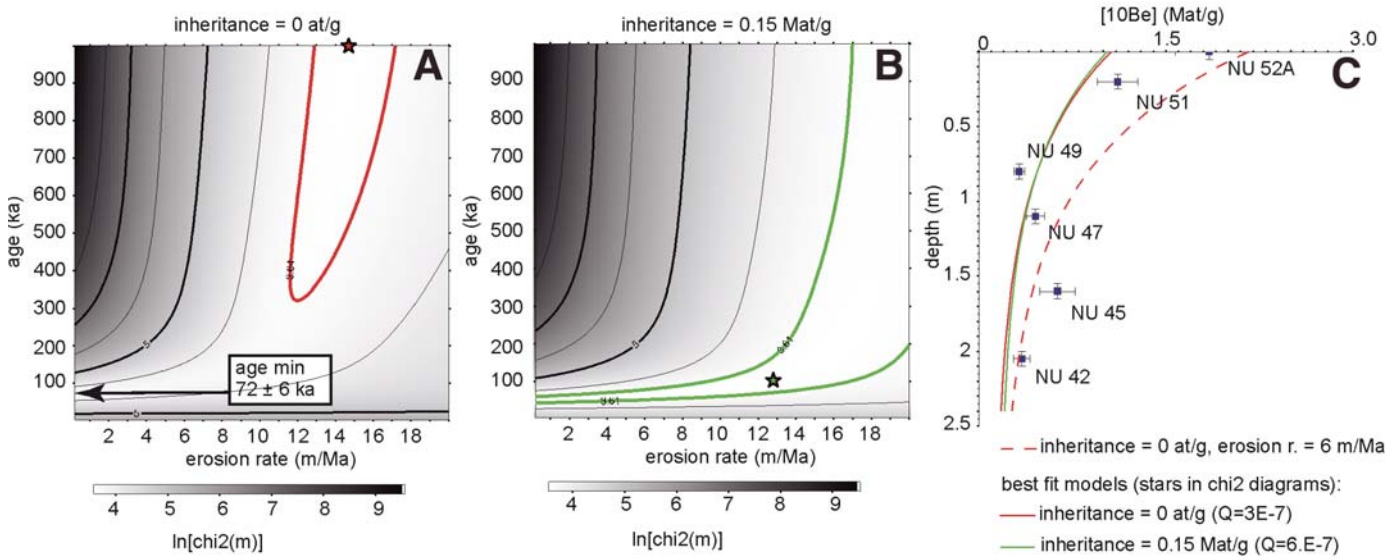

Figure 12. Results of the ^{10}Be analysis on surface S1 in Noyan Uul. A and B: Plots of the results of the chi-square inversion. Stars represent the best-fit solutions, and colored curve defines the associated 1σ uncertainties. The inversion gives a minimum age of 72 ± 6 ka for the model with no inheritance and 50 ± 8 ka for the model with 0.15 M atoms/g of inheritance. C: Plot of the ^{10}Be concentration of the samples along the depth profile and best-fit theoretical models issued from the chi-square inversion.

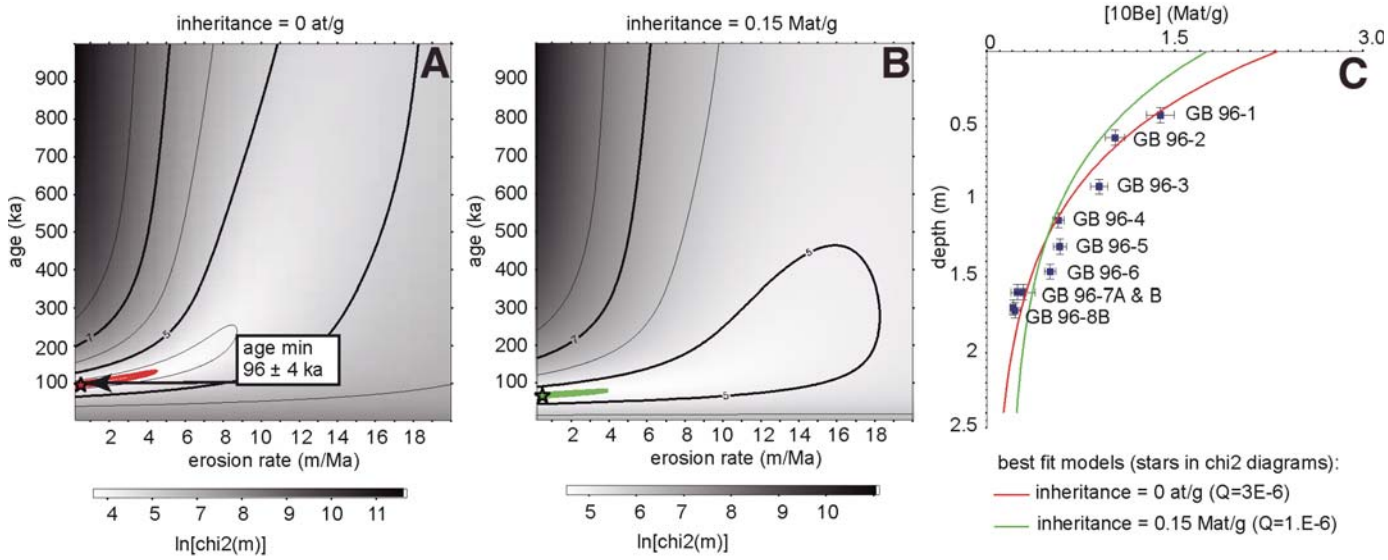

Figure 13. Results of the ^{10}Be analysis on surface S2 in the western fan (central part of the Gurvan Bulag thrust fault). A and B: Plots of the results of the chi-square inversion, giving a minimum age of 96 ± 4 ka for the model with no inheritance and 66 ± 2 ka for the model with 0.15 M atoms/g of inheritance. C: Plot of the ^{10}Be concentration of the samples along the depth profile and best-fit theoretical models issued from the chi-square inversion.

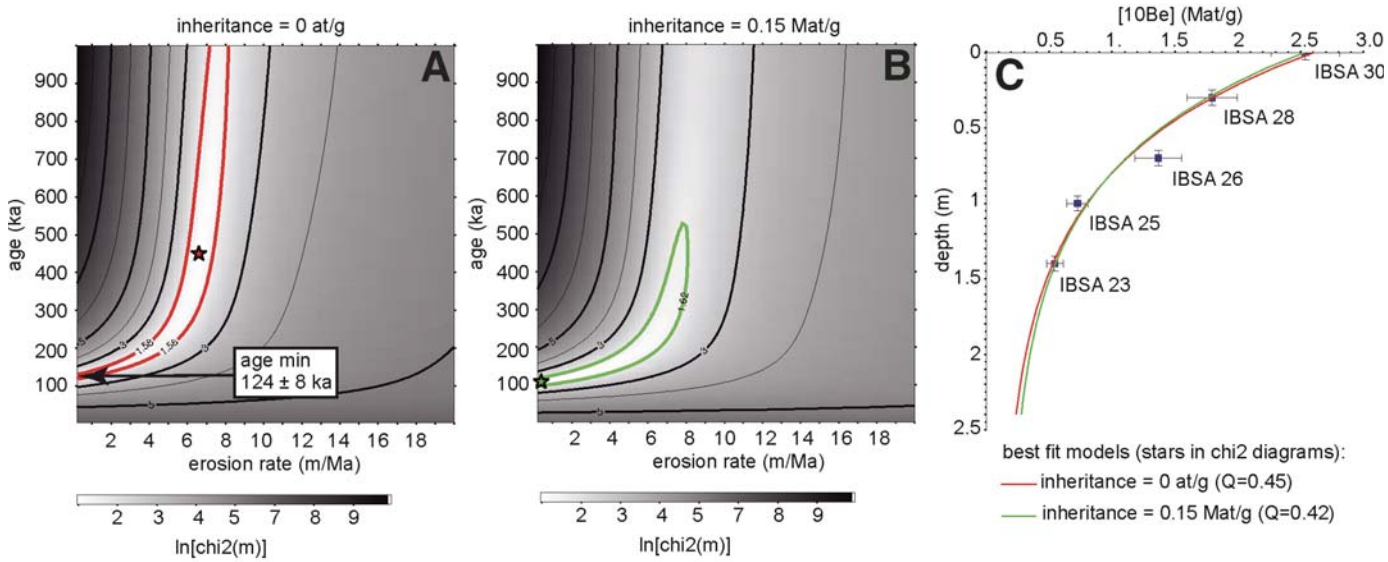

Figure 14. Results of the ^{10}Be analysis on surface S2 in the eastern fan (central part of the Gurvan Bulag thrust fault). A and B: Plots of the results of the chi-square inversion, giving a minimum age of 124 ± 8 ka for the model with no inheritance and 106 ± 6 ka for the model with 0.15 M atoms/g of inheritance. C: Plot of the ^{10}Be concentration of the samples along the depth profile and best-fit theoretical models issued from the chi-square inversion.

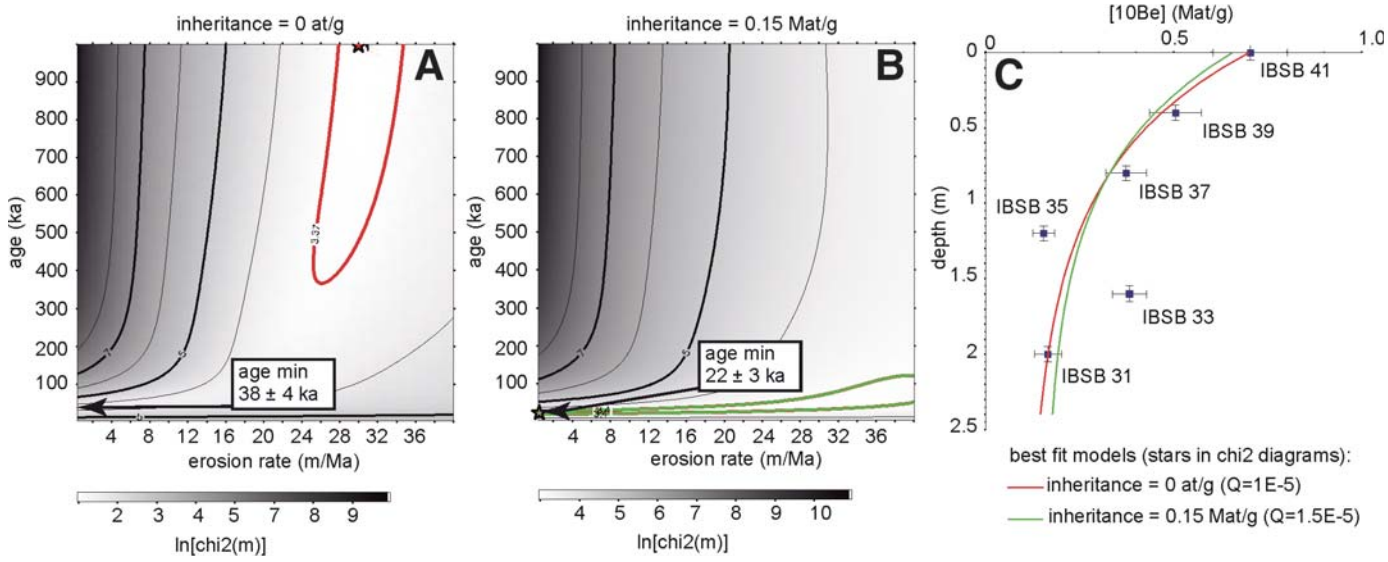

Figure 15. Results of the ^{10}Be analysis on surface S3 in the eastern fan (central part of the Gurvan Bulag thrust fault). A and B: Plots of the results of the chi-square inversion, giving a minimum age of 38 ± 4 ka for the model with no inheritance and 22 ± 3 ka for the model with 0.15 M atoms/g of inheritance. C: Plot of the ^{10}Be concentration of the samples along the depth profile and best-fit theoretical models issued from the chi-square inversion.

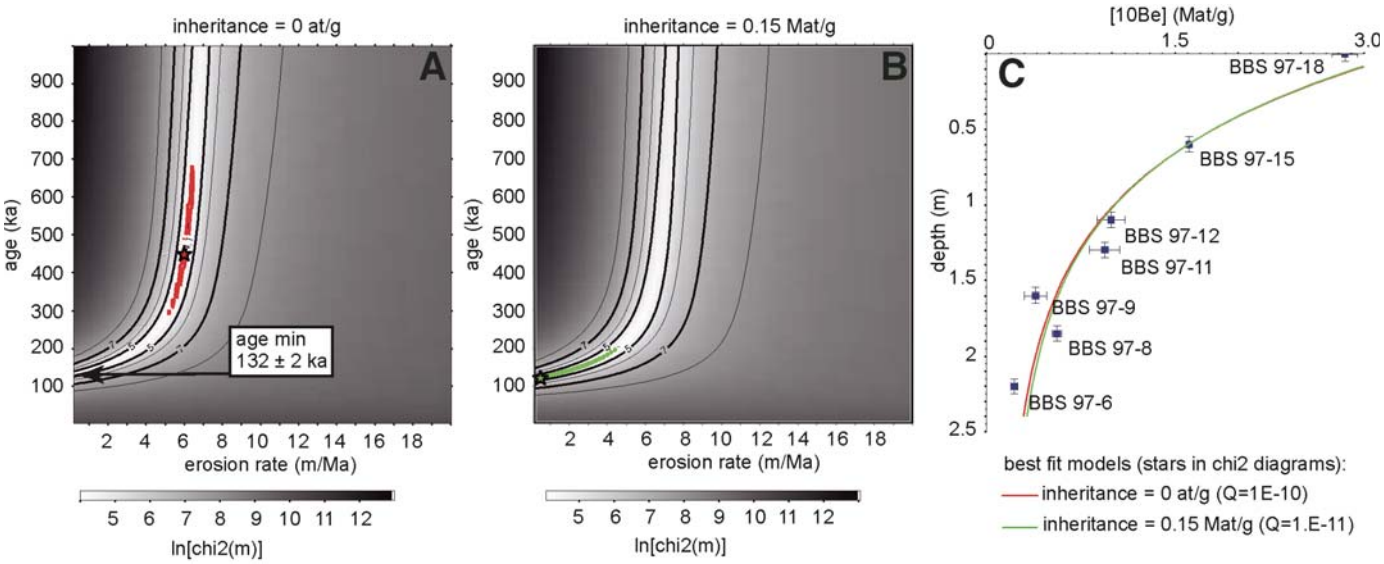

Figure 16. Results of the ^{10}Be analysis on surface S1 at the studied site (Baga Bogd thrust fault). A and B: Plots of the results of the chi-square inversion, giving a minimum age of 132 ± 2 ka for the model with no inheritance and 120 ± 2 ka for the model with 0.15 M atoms/g of inheritance. C: Plot of the ^{10}Be concentration of the samples along the depth profile and best-fit theoretical models issued from the chi-square inversion.

Samples with concentrations approaching steady-state values do not yield exposure ages. Thus, we chose to estimate the ages corresponding to models for no inheritance and no erosion. These ages a priori correspond to minimum ages, although increase of apparent age by inheritance is possible for the young surface S3 at Gurvan Bulag. On the time versus erosion rate diagrams, ages are given by the minimum of the chi-square value on the *y*-axis (erosion rate = 0). Uncertainties correspond to a confidence interval of 1σ. The minimum ages obtained are 72 ± 6 ka for S1 at Noyan Uul (Fig. 12); 96 ± 4 ka for S2 on the western fan at Gurvan Bulag (Fig. 13), 124 ± 8 ka for S2 (Fig. 14) and 38 ± 4 ka for S3 (Fig. 15) on the eastern fan at the same site; 132 ± 2 ka for S1 at the south of Baga Bogd (Fig. 16).

Surficial Boulders

The reevaluation of surface exposure ages using the ^{10}Be concentrations on surficial boulders (see the penultimate paragraph of the section "Dating Morphotectonic Markers" and Tables 1–3) gives the following results: At Noyan Uul, the reevaluation of the exposure age of the surface S1 gives 61.8 $^{+14.9}/_{-4.7}$ ka. At Gurvan Bulag, within the western fan, exposure ages for surfaces S2, S3, and S4 are 128.7 $^{+15.1}/_{-26.5}$ ka, 14.3 $^{+12.6}/_{-4.1}$ ka, and 4.6 $^{+5.4}/_{-1.8}$ ka, respectively. The age found on S3 was also found in samples collected at a depth ≥2 m in a recent debris flow S5 (15.6 $^{+3.7}/_{-4.0}$ ka) inset in the S4 surface reworking upstream and previously exposed material. At Baga Bogd, the reevaluation of the exposure ages for the surface S3 gives 20.2 $^{+3.7}/_{-3.7}$ ka.

Concluding Remarks on Reevaluated ^{10}Be Ages

For the old fans (surface S1 at Noyan Uul, surface S2 at Gurvan Bulag), minimum ages estimated using surficial boulders or depth profiles (with or without inheritance) are consistent for a given surface. On the other hand, the age of the young surfaces (S3 at Gurvan Bulag and at Baga Bogd) determined using surficial boulders is more consistent with the age given by the modeling of the depth profile of S3 at Gurvan Bulag that takes into account 0.15 M atoms/g of inheritance (Fig. 15B). Because exposure ages calculated from profiles on young surfaces are highly sensitive to inheritance, and considering the larger sample population of surficial boulders, we suggest an age of ca. 20 ka for S3.

RECALCULATION OF SLIP RATES

Taking into account the measured offsets and the reevaluated exposure ages (for all sites, we use ages obtained from the depth profiles except at Gurvan Bulag for surface S3, where we used the weighted mean age obtained from surficial samples collected within the western fan), we calculated fault slip rates (with uncertainties incorporating errors in ages as well as in offsets) during the Late Pleistocene–Holocene within the Gurvan Bogd fault system (Fig. 17).

At Noyan Uul, the left-lateral displacement of 110 ± 10 m and the minimum age of 72 ± 6 ka for surface S1 yield a maximum horizontal slip rate of the Bogd fault of 1.55 ± 0.26 mm/yr during the Late Pleistocene–Holocene.

At Gurvan Bulag, we estimated vertical slip rates over two periods of time, the past ~100–130 k.y. and the past ~20 k.y.,

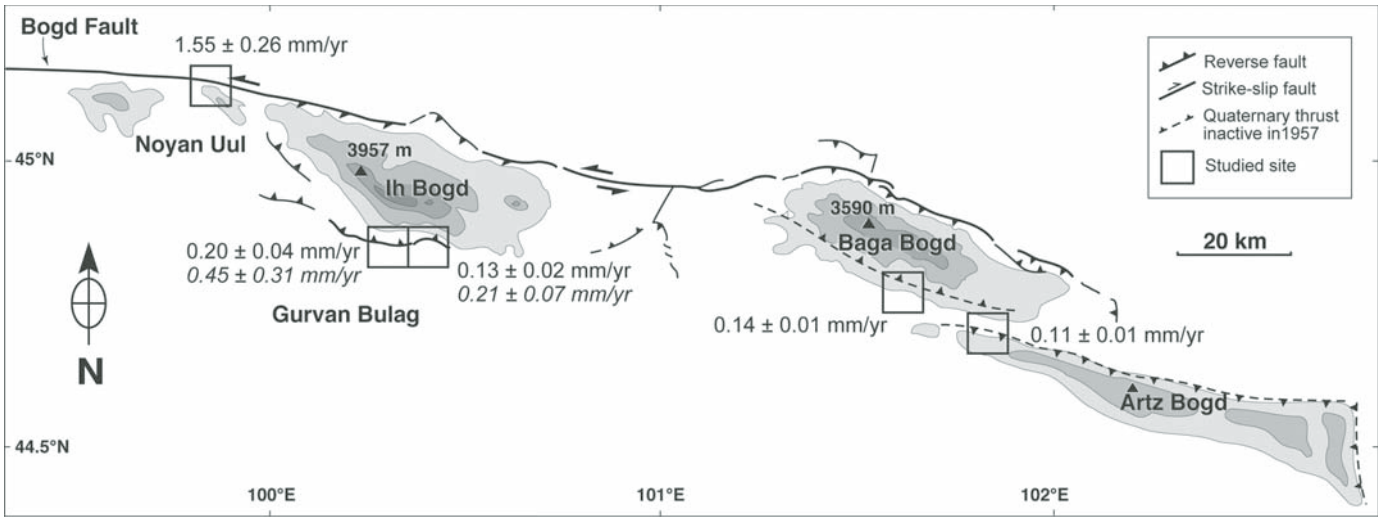

Figure 17. Reestimated maximum fault slip rates within the Gurvan Bogd fault system. All the slip rates are vertical ones, except at Noyan Uul, and calculated for the Late Pleistocene–Holocene. At Gurvan Bulag, the rates in italics are calculated for the past ~15–20 k.y.

from the two main offset surfaces S2 and S3 observed within the two fans. Because it cannot be determined when surfaces formed during the seismic cycle, the Late Pleistocene–Holocene slip rates were bracketed using the mean total offset of surfaces and the mean total offset of surfaces less the mean 1957 offset. On the basis of earlier work (Prentice et al., 2002), we estimated the mean 1957 offset at ~1.5 m within the western fan and ~1 m within the eastern fan. Dividing these bracketed offsets by the surface age yields upper and lower limits on the vertical slip rate. Within the western fan, over the past ~100 k.y., the slip-rate upper and lower limits are 0.21 ± 0.03 mm/yr and 0.19 ± 0.03 mm/yr, respectively. For the past ~20 k.y., the slip-rate upper and lower limits are 0.48 ± 0.28 mm/yr and 0.37 ± 0.23 mm/yr, respectively, considering an offset of 6.5 ± 1.2 m. They increase to 1.18 ± 0.55 mm/yr and 1.08 ± 0.51 mm/yr, respectively, assuming an offset of 17.3 ± 0.4 m. Within the eastern fan, vertical slip-rate upper and lower limits are 0.13 ± 0.01 mm/yr and 0.12 ± 0.01 mm/yr, respectively, for the past ~130 k.y., and 0.23 ± 0.05 mm/yr and 0.19 ± 0.05 mm/yr, respectively, for the past ~20 k.y.

Vertical slip rates estimated on both fans are consistent if we assume that within the western fan, the S3 debris flow was deposited on a preexisting offset morphology: the S2 surface that was already incised by gullies S4. Consequently the age of S4 should be the same as that of S3. This is not inconsistent with ages reported for S4; one of the five S4 samples (MO95-20) yields an age of 15.4 ± 1.5 ka, consistent with the age of the S3 debris flow (Ritz et al., 2003). It may have been deposited on S4 when the debris flow S3 was deposited atop surface S2. Under this scenario the younger exposure ages ($4.6\ ^{+5.4}/_{-1.8}$ ka) of the other four S4 samples would represent the results of complex exposure histories, including delivery to the surface by erosion of adjacent slopes.

At South Baga Bogd, the vertical offset of 19.0 ± 0.5 m measured across the scarp and the minimum age of 132 ± 2 ka given by the model for surface S2 yield a maximum vertical slip rate of 0.14 ± 0.01 mm/yr during the Late Pleistocene–Holocene.

At Artz Bogd, surface incision by the drainage network clearly postdates the vertical displacement (20.3 ± 0.5 m) of the deposits. For a minimum age of the upper deposit of 181 ± 12 ka, this yields a maximum vertical slip rate of 0.11 ± 0.01 mm/yr.

SLIP RATES AND RECURRENCE INTERVALS OF EARTHQUAKES WITHIN THE GURVAN BOGD FAULT SYSTEM

It is possible to compare the 1957 dislocation along the main left-lateral strike-slip Bogd fault with dislocations associated with the penultimate earthquake and earlier events. Our morphotectonic study of two sites demonstrates that features (offset streams or shutter ridges) offset during the 1957 event also show well-preserved pre-1957 offsets corresponding to one or more previous events. Digital elevation models of these sites show dislocations that are multiples of the 1957 dislocation. At Noyan Uul, we measured constant dislocation of 5.25 ± 0.25 m (Fig. 18), and at north of Ih Bogd, where the slip is oblique along the fault, we measured several horizontal components that were all multiples of 3 m (Ritz, 2003). This suggests that the successive dislocations along the Bogd fault have the same magnitude and can be defined as characteristic dislocations (e.g., Schwartz and Coppersmith, 1984; Sieh, 1996). Coupled with knowledge of average slip rate, this allows estimation of the return period. At Noyan Uul, for instance, dividing the characteristic dislocation (~5.25 m) by the maximum slip rate (1.55 ± 0.26 mm/yr) yields a minimum average recurrence interval of 3000–4000 yr.

At Gurvan Bulag, the amount of vertical offset for the 1957 is more difficult to establish (see above) and, a fortiori, we do not have estimates of earlier dislocations, so estimation of recurrence

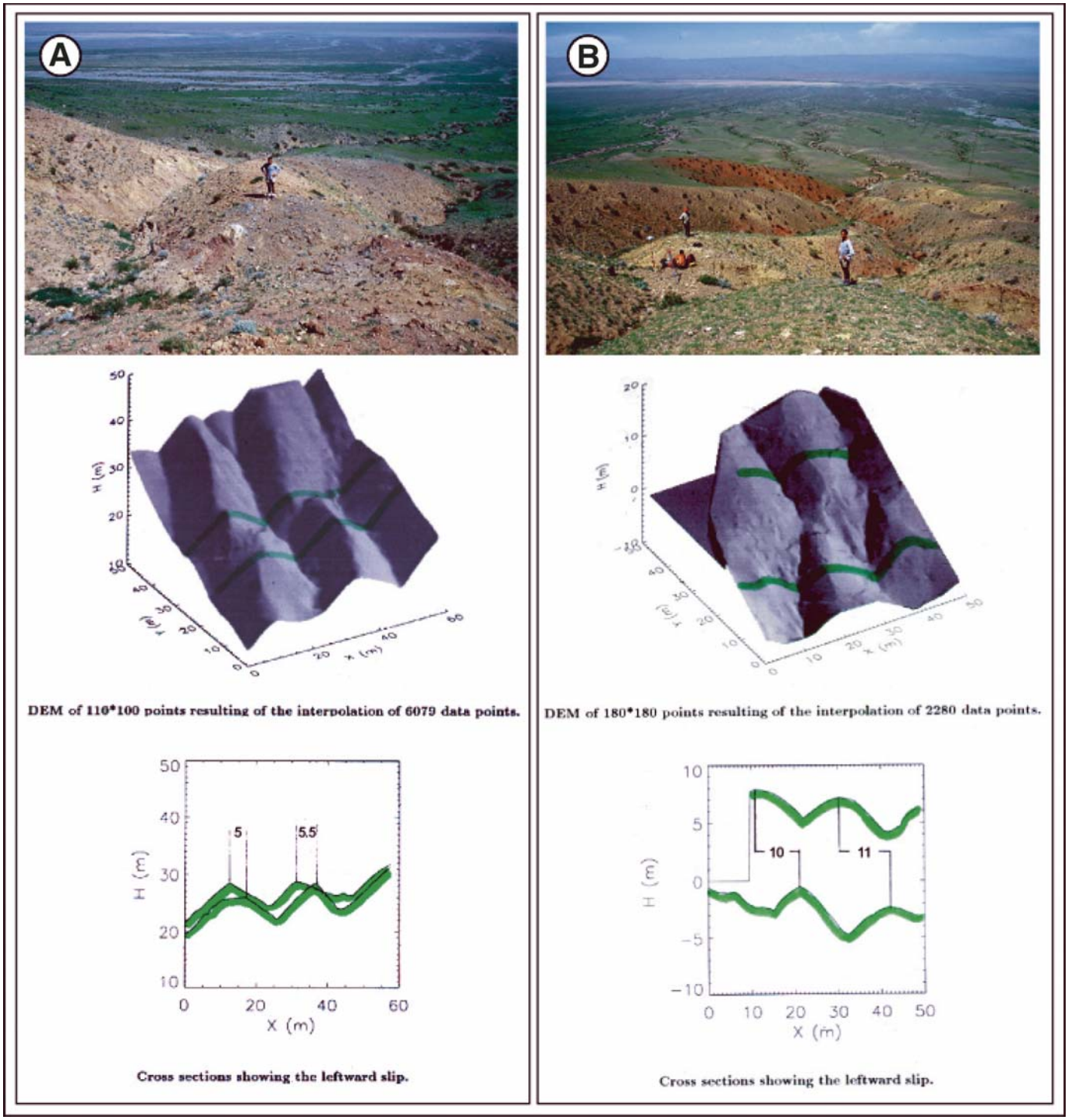

Figure 18. Examples of shutter ridges and streams along the Bogd fault at Noyan Uul with field picture, corresponding digital elevation model, and cross sections. A: 1957 dislocation. B: Dislocation twice the 1957 displacement.

intervals from dating offset markers is problematic. However, paleoseismic investigations (Prentice et al., 2002) indicate an average periodicity of ~3600 yr, similar to that reported for the Bogd fault. This suggests that the two faults may have ruptured simultaneously during earlier events, as they did in 1957, although the paleoseismic data clearly indicate that this was not the case for the penultimate event (Prentice et al., 2002). The hypothesis of a general pattern of simultaneous rupture is also supported by the overall correspondence between the 1957 fault patterns (geometry, kinematics, magnitudes of dislocations) and the topography of the Gurvan Bogd mountain range.

ALLUVIAL SURFACES DEPOSITION AND THEIR EVOLUTION THROUGH TIME IN GOBI-ALTAY: CONSEQUENCES IN TERMS OF SAMPLING STRATEGY

Compilation of morphotectonic studies of the Gurvan Bogd mountain range leads to several conclusions on the history and evolution of alluvial surfaces within the arid climate of Gobi-Altay. ^{10}Be dates suggest the occurrence of episodes of significant aggradation localized in time. Even though the old surface (S1) in Noyan Uul on the northern flank of the Ih Bogd massif appears younger than the two old surfaces in the southern flank (S2 at Gurvan Bulag and S1 at Baga Bogd), it is likely that the three surfaces are associated with the same climatic pulse. Indeed, the morphology on both sides clearly shows that episodes of alluviation are separated by long periods of drought. It is therefore difficult to imagine that the pulses that controlled the alluviation within the Gurvan Bogd massifs were different from one flank to another. Furthermore, Hanks et al. (1997) found another ca. 100 ka alluvial fan along the northern flank of the Ih Bogd massif. Therefore, we believe that the observed differences in the minimum ages are associated with greater postdepositional perturbation of surfaces on the northern flank. Despite the uncertainties inherent in cosmic-ray exposure ages, our results suggest that the two last pulses could have been contemporaneous with global climate changes at the terminations of marine isotope stages (MIS) 2 and 6, and can be interpreted as the effects of major alluvial events due to enhanced stream power reworking the material that accumulated in the slopes or in the drainage network of the upstream basins during drier and colder periods.

Taking into account the exposure ages of the surfaces and their morphologies, our study also enables us to outline the evolution of the geomorphic surfaces and their associated deposits (Fig. 19): Fan surfaces evolve from a bar-and-swale morphology characterized by a high-frequency/low-amplitude topographic signal totally covered by boulder fields (with different sizes of boulders) toward a low-frequency/high-amplitude topographic signal on which the number of standing boulders diminishes gradually. Eventually, the surfaces become flat with no more boulders remaining. This scenario suggests that the erosion rate of the boulders gradually catches up to the rate of removal of fine-grained material on the surface. In the Gurvan Bogd mountain range, this stage appears to be reached after ~100 k.y.

The foregoing observations allow development of sampling strategy for such context: In all cases, because of the potential of inheritance and of complex postdepositional history—especially when studying stepped markers—it is useful to study the distribution of ^{10}Be concentrations at depth, especially when the surface is young. This allows determination of a minimum surface age corrected for preexposure. To get closer to the true age, this protocol can be combined with a statistical analysis of surface concentrations on top of the remaining boulders—if any—that are well embedded in surfaces.

CONCLUSIONS

This article reviews age estimates of faulted morphological markers along the Gurvan Bogd fault system, and documents climatic and tectonic processes in eastern Gobi-Altay. These results suggest episodes of aggradation occurring at the times of major global climatic changes at ca. 15–20 ka and ca. 100–130 ka, and provide evidence for another much earlier aggradational episode occurring before 400 ka.

Dating alluvial surfaces and calculation of their offsets permitted quantification of slip rates along the fault segments bounding the Gurvan Bogd fault system. The main fault, the Bogd fault, has a maximum horizontal left-lateral slip rate of ~1.5 mm/yr during the Late Pleistocene–Holocene, consistent with the present-day slip rate estimated from GPS measurements (Calais et al., 2003). Segments of reverse faulting along the Gurvan Bogd fault system have vertical slip rates between 0.1 and 0.2 mm/yr during the past ~100–130 k.y. At Gurvan Bulag, the activity of the fault appears to have increased slightly since ca. 15–20 ka. Characteristic dislocations observed along the Bogd fault suggest return periods of earthquakes similar to 1957 between 3000 and 4000 yr. If we extrapolate the Late Pleistocene–Holocene rates to a longer period of time, the uplift of the summit erosional surface of the Ih Bogd massif (the difference in height between the summit surface and the bounding faults being ~2000 m) would have begun between 10 and 20 Ma. When compared with the 0.2–0.3 mm/yr uplift rate of the Ih Bogd massif estimated from dating of strath terraces in the Bitut River (Vassallo et al., 2004), our results suggest that the thrust faults that we studied do not fully account for the uplift of the Gurvan Bogd massif. This is consistent with the suggestion of Bayasgalan et al. (1999a) that other thrust faults also contribute to the uplift.

ACKNOWLEDGMENTS

This paper is a review of several studies in Gobi-Altay since 1992. Seven expeditions involving a total of five months of fieldwork were undertaken in collaboration with the Center of Informatic and Remote Sensing; the Mongolian University of Science and Technology, Ulaanbataar; the Bullard Laboratories, Cambridge, UK; the U.S. Geological Survey, Menlo Park;

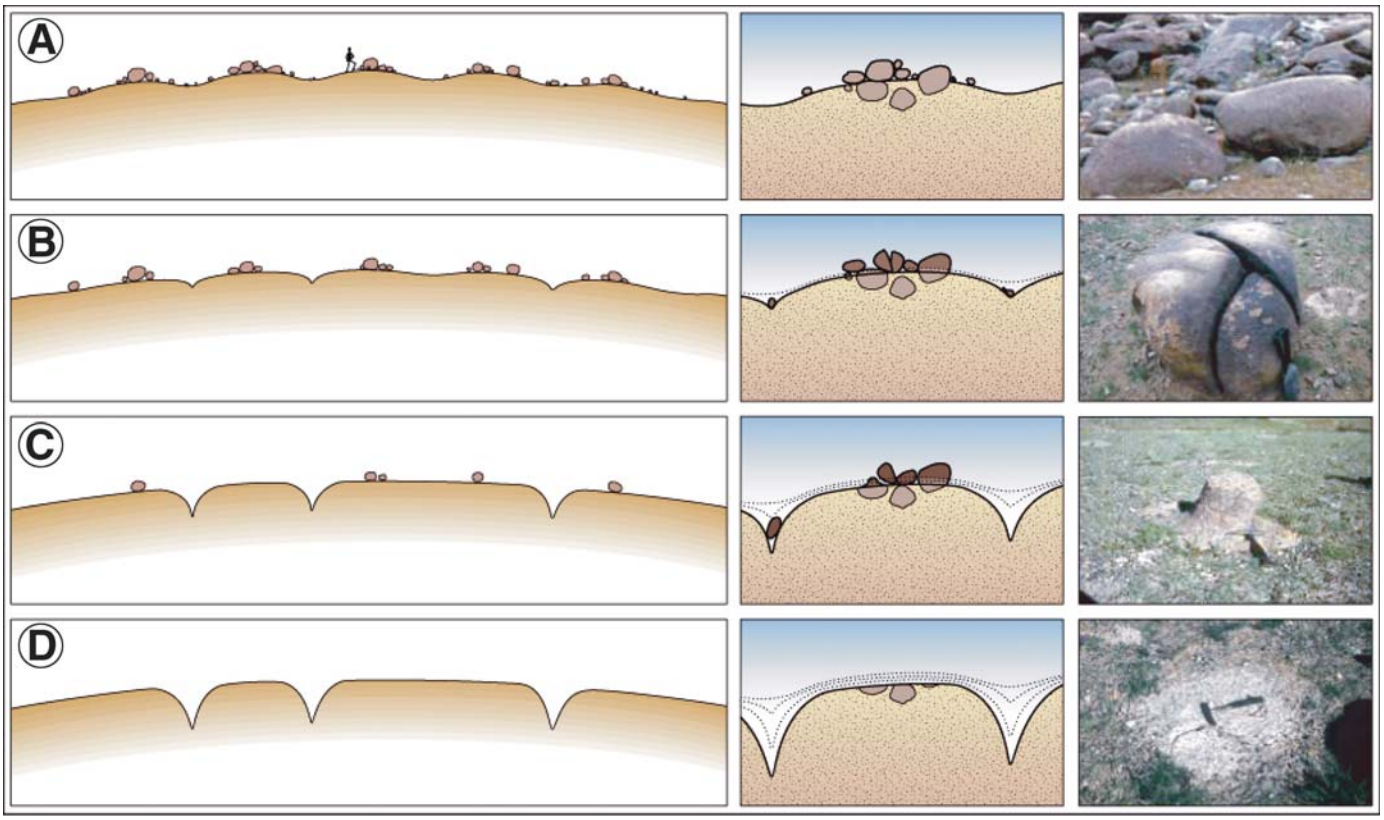

Figure 19. Scenario of the evolution of an alluvial fan surface abandoned after its displacement along a fault. A: "Bar-and-swale" morphology with largest boulders along bars. B: Smoothing of bars by collapse of boulders and diffusion of finer material (boulders are weathered and fissured). C: The surface gets gradually flatter and more incised (few hard-core boulders still stand on the surface). D: The surface is totally flattened with deep incisions (phantoms of boulders are eroded at the same erosion rate as the surface).

and the LLNL, Livermore. We thank again A. Bayasgalan, K. Berryman, E. Calais, J. Deverchères, B. Enhtuvshin, R. Finkel, P. Galsan, M. Ganzorig, T. Hanks, J. Jackson, K. Kendrick, H. Philip, C. Prentiss, G. Raisbeck, A. Schlupp, D. Schwartz, M. Todbileg, and F. Yiou for fruitful discussions. Many thanks to Anne Delplanque for the drawings. We acknowledge L. Siame and an anonymous referee for their reviews that helped us to improve the original manuscript.

REFERENCES CITED

Anderson, R.S., Repka, J.L., and Dick, G.S., 1996, Explicit treatment of inheritance in dating depositional surfaces using in situ ^{10}Be and ^{26}Al: Geology, v. 24, p. 47–51, doi: 10.1130/0091-7613(1996)024<0047:ETOIID>2.3.CO;2.

Baljinnyam, I., Bayasgalan, A., Borisov, B.A., Cisternas, A., Dem'yanovich, M.G., Ganbaatar, L., Kochetkov, V.M., Kurushin, R.A., Molnar, P., Philip, H., and Vashchilov, Yu.Ya., 1993, Ruptures of major earthquakes and active deformation in Mongolia and its surroundings: Geological Society of America Memoir 181, 62 p.

Bayasgalan, A., 1999, Active tectonics of Mongolia [Ph.D. thesis]: Cambridge, UK, University of Cambridge, 182 p.

Bayasgalan, A., Jackson, J., Ritz, J.-F., and Carretier, S., 1999a, Field examples of strike-slip fault terminations in Mongolia and their tectonic significance: Tectonics, v. 18, p. 394–411, doi: 10.1029/1999TC900007.

Bayasgalan, A., Jackson, J., Ritz, J.-F., and Carretier, S., 1999b, "Forebergs", flowers structures, and the development of large intra-continental strike-slip fault: The Gurvan Bogd fault system in Mongolia: Journal of Structural Geology, v. 21, p. 1285–1302, doi: 10.1016/S0191-8141(99)00064-4.

Bierman, P.R., 1994, Using in situ produced cosmogenic isotopes to estimate rates of landscape evolution: A review from the geomorphic perspective: Journal of Geophysical Research, v. 99, p. 13,885–13,896, doi: 10.1029/94JB00459.

Bierman, P.R., Gillespie, A.R., and Caffee, M.W., 1995, Cosmogenic ages for earthquakes recurrence intervals and debris flow fan deposition, Owen valley, California: Science, v. 270, p. 447–450.

Braucher, R., Brown, E.T., Bourlès, D.L., and Colin, F., 2003, In situ produced ^{10}Be measurements at great depths: Implications for production rates by fast muons: Earth and Planetary Science Letters, v. 211, p. 251–258, doi: 10.1016/S0012-821X(03)00205-X.

Brown, E.T., Edmond, J.M., Raisbeck, G.M., Yiou, F., Kurz, M.D., and Brook, E.J., 1991, Examination of surface exposure ages of Antarctic moraines using in situ produced ^{10}Be et ^{26}Al: Geochimica et Cosmochimica Acta, v. 55, p. 2269–2283, doi: 10.1016/0016-7037(91)90103-C.

Brown, E.T., Brook, E.J., Raisbeck, G.M., Yiou, F., and Kurz, M.D., 1992, Effective attenuation lengths of cosmic rays producing ^{10}Be and ^{26}Al in quartz: Implication for exposure age dating: Geophysical Research Letters, v. 19, no. 4, p. 369–372.

Brown, E.T., Bourlès, D.L., Colin, F., Raisbeck, G.M., Yiou, F., and Desgarceaux, S., 1995, Evidence for muon-induced in situ production of ^{10}Be in near-surface rocks from the Congo: Geophysical Research Letters, v. 22, p. 703–706, doi: 10.1029/95GL00167.

Brown, E.T., Bendick, R., Bourlès, D.L., Gaur, V., Molnar, P., Raisbeck, G.M., and Yiou, F., 2002, Slip rates of the Karakorum fault, Ladakh, India, determined using cosmic ray exposure dating of debris flows and

moraines: Journal of Geophysical Research, v. 107, no. B9, p. 2192, doi: 10.1029/2000JB000100.

Bucknam, R.C., and Anderson, R.E., 1979, Estimation of fault-scarp ages from a scarp-height-slope-angle relationship: Geology, v. 7, p. 11–14, doi: 10.1130/0091-7613(1979)7<11:EOFAFA>2.0.CO;2.

Burbank, D.W., and Anderson, R.S., 2001, Tectonic geomorphology: Malden, USA, Blackwell Science, 274 p.

Calais, E., Vergnolle, M., Sankov, V., Lukhnev, A., Miroshnitchenko, A., Amarjargal, S., and Dervèrchère, J., 2003, GPS measurements of crustal deformation in the Baikal-Mongolia area (1994–2002): Implications on current kinematics of Asia: Journal of Geophysical Research, v. 108, no. B10, p. 2501, doi: 10.1029/2002JB002373.

Carretier, S., 2000, Cycle sismique et surrection de la chaîne de Gurvan Bogd (Mongolie): Approche de la géomorphologie quantitative [Ph.D. thesis]: Université de Montpellier 2, 324 p.

Carretier, S., Lucazeau, F., and Ritz, J.-F., 1998, Approche numérique des intéractions entre climat, faille active et érosion: Compte Rendus Academie Sciences Paris, v. 326, p. 391–397.

Carretier, S., Ritz, J.F., Jackson, J., and Bayasgalan, A., 2002, Morphological dating of cumulative reverse fault scarp: Examples from the Gurvan Bogd fault system, Mongolia: Geophysical Journal International, v. 148, p. 256–277, doi: 10.1046/j.1365-246X.2002.01599.x.

Cunningham, D.W., 1998, Lithospheric controls on late Cenozoic construction of the Mongolian Altai: Tectonics, v. 17, p. 891–902, doi: 10.1029/1998TC900001.

Cunningham, D.W., Windley, B.F., Dorjnamjaa, D., Badamgarov, G., and Saandar, M., 1996, A structural transect across the Mongolian western Altai: Active transpressional mountain building in central Asia: Tectonics, v. 15, p. 142–156, doi: 10.1029/95TC02354.

Cunningham, D.W., Windley, B.F., Owen, L.A., Barry, T., Dorjnamjaa, D., and Badamgarav, J., 1997, Geometry and style of partitioned deformation within a late Cenozoic transpressional zone in the eastern Gobi Altai Mountains, Mongolia: Tectonophysics, v. 277, p. 285–306, doi: 10.1016/S0040-1951(97)00034-6.

Davis, J.C., Proctor, I.D., Southon, J.R., Caffee, M.W., Heikkinen, D.W., Roberts, M.L., Moore, T.L., Turtletaub, K.W., Nelson, D.E., Loyd, D.H., and Vogel, J.S., 1990, Lawrence Livermore National Laboratory–University of California Center for Accelerator Mass Spectrometry facility and research program: Nuclear Instruments and Methods in Physics Research, B52, p. 269–272.

Florensov, N.A., and Solonenko, V.P., editors, 1965, The Gobi-Altay earthquake: Washington, D.C., U.S. Department of Commerce, 424 p.

Hancock, G.S., Anderson, R.S., Chadwick, O.A., and Finkel, R.C., 1999, Dating fluvial terraces with ^{10}Be and ^{26}Al profiles: Application to the Wind River, Wyoming: Geomorphology, v. 27, p. 41–60, doi: 10.1016/S0169-555X(98)00089-0.

Hanks, T., Ritz, J.-F., Kendrick, K., Finkel, R.C., and Garvin, C.D., 1997, Uplift rates in a continental interior: Faulting offsets of a ~100 ka abandoned fan along the Bogd fault, southern Mongolia: Proceedings of the Penrose Conference on the Tectonics of Continental Interiors, 23–28 September 1997, Cedar City, Utah.

Hanks, T.C., Bucknam, R.C., Lajoie, K.R., and Wallace, R.E., 1984, Modification of wave-cut and faulting-controlled landforms: Journal of Geophysical Research, v. 89, p. 5771–5790.

Klein, J., Giegengack, R., Middleton, R., Sharma, P., Underwood, J.R., and Weeks, R.A., 1986, Revealing histories of exposure using in situ produced ^{26}Al and ^{10}Be in Libyan Desert Glass: Radiocarbon, v. 28, no. 2A, p. 547–555.

Kurushin, R.A., Bayasgalan, A., Ölziybat, M., Enkhtuvshin, B., Molnar, P., Bayarsayhan, C., Hudnut, K.W., and Lin, J., 1997, The surface rupture of the 1957 Gobi-Altay, Mongolia, earthquake: Geological Society of America Special Paper 320, 143 p.

Meriaux, A.S., Ryerson, F.J., Tapponnier, P., Van der Woerd, J., Finkel, R.C., Xiwei Xu, Zhiqin Xu, and Caffee, M.W., 2004, Rapid slip along the central Altyn Tagh fault: Morphochronologic evidence from Cherchen He and Sulamu Tagh: Journal of Geophysical Research, v. 109, B06401, doi: 10.1029/2003JB002556.

Meriaux, A.S., Tapponnier, P., Ryerson, F.J., Xu Xiwei, King, G., Van der Woerd, J., Finkel, R.C., Li Haibing, Caffee, M.W., Xu Zhiqin, and Chen Wenbin, 2005, The Aksay segment of the northern Altyn Tagh fault: Tectonic geomorphology, landscape evolution, and Holocene slip rate: Journal of Geophysical Research, v. 110, B04404, doi: 10.1029/2004JB003210.

Molnar, P., and Tapponnier, P., 1975, Cenozoic tectonics of Asia: Effects of a continental collision: Science, v. 189, p. 419–426.

Molnar, P., and D. Qidong, 1984, Faulting associated with large earthquakes and the average rate of deformation in Central and eastern Asia: Journal of Geophysical Research, v. 89, p. 6203–6227.

Nishiizumi, K., Lal, D., Klein, J., Middleton, R., and Arnold, J.R., 1986, Production of ^{10}Be and ^{26}Al by cosmic rays in terrestrial quartz in situ and implications for erosion rates: Nature, v. 319, p. 134–135, doi: 10.1038/319134a0.

Owen, L.A., Cunningham, D.W., Richards, B.W., Rhodes, E., Windley, B.F., Dorjnamjaa, D., and Badamgarav, J., 1999, Timing of formation of forebergs in the northeastern Gobi-Altai, Mongolia: Implications for mountain uplift rates and earthquake recurrence intervals: Geological Society [London] Journal, v. 156, p. 457–464.

Prentice, C., Kendrick, K., Berryman, K., Bayasgalan, A., Ritz, J.F., and Spencer, J.Q., 2002, Prehistoric ruptures of the Gurvan Bulag fault, Gobi Altay, Mongolia: Journal of Geophysical Research, v. 107, p. 2321, doi: 10.1029/2001JB000803.

Press, W.H., Teukolsky, S.A., Vetterling, W.T., and Flannery, B.P., 1996, Numerical recipes in Fortran 90—The art of parallel scientific computing: Cambridge, UK, Cambridge University Press, 1356 p.

Raisbeck, G.M., Yiou, F., Bourlès, D.L., Lestringuez, J., and Deboffe, D., 1987, Measurements of ^{10}Be and ^{26}Al with a Tandetron AMS facility: Nuclear Instruments and Methods in Physics Research, v. 29, p. 22–26, doi: 10.1016/0168-583X(87)90196-0.

Raisbeck, G.M., Yiou, F., Bourlès, D.L., Brown, E.T., Deboffle, D., Jouhanneau, P., Lestringuez, J., and Zhou, Z.Q., 1994, The AMS facility at Gif-sur-Yvette: Progress, perturbations and projects: Nuclear Instruments and Methods in Physics Research, v. 92, p. 43–46, doi: 10.1016/0168-583X(94)95972-2.

Repka, J.L., Anderson, R.S., and Finkel, R.C., 1997, Cosmogenic dating of fluvial terraces, Fremont River, Utah: Earth and Planetary Science Letters, v. 152, no. 1-4, p. 59–73.

Ritz, J.F., 2003, Analyse de la tectonique active en domaine continental: Approche morphotectonique et paléosismologique [HDR thesis]: Université de Montpellier 2, V1, 72 p.

Ritz, J.F., Brown, E.T., Bourlès, D.L., Philip, H., Schlupp, A., Raisbeck, G.M., Yiou, F., and Enkhtuvshin, B., 1995, Slip rates along active faults estimated with cosmic-ray-exposure dates: Application to the Bogd fault, Gobi-Altaï, Mongolia: Geology, v. 23, p. 1019–1022, doi: 10.1130/0091-7613(1995)023<1019:SRAAFE>2.3.CO;2.

Ritz, J.F., Bourlès, D., Brown, E.T., Carretier, S., Chery, J., Enhtuvushin, B., Galsan, P., Finkel, R.C., Hanks, T.C., Kendrick, K.J., Philip, H., Raisbeck, G., Schlupp, A., Schwartz, D.P., and Yiou, F., 2003, Late Pleistocene to Holocene slip rates for the Gurvan Bulag thrust fault (Gobi-Altay, Mongolia) estimated with ^{10}Be dates: Journal of Geophysical Research, v. 108, no. B3, p. 2162, doi: 10.1029/2001JB000553.

Schlupp, A., 1996, Néotectonique de la Mongolie Occidentale analysée à partir de données de terrain, sismologiques et satellitaires [Ph.D. thesis]: Strasbourg, University Louis Pasteur, 172 p.

Schwartz, D., and Coppersmith, K., 1984, Fault behavior and characteristic earthquakes: Examples from the Wasatch and San Andreas faults: Journal of Geophysical Research, v. 89, p. 5681–5698.

Siame, L., Braucher, R., and Bourlès, D., 2000, Les nucléides cosmogéniques produits in situ: de nouveaux outils en géomorphologie quantitative: Bulletin de la Société Géologique de France, v. 171, p. 383–396, doi: 10.2113/171.4.383.

Siame, L., Bellier, O., Braucher, R., Sébrier, M., Cushing, M., Bourlès, D., Hamelin, B., Baroux, E., de Voogd, B., Raisbeck, G., and Yiou, F., 2004, Local erosion rates versus active tectonics: Cosmic ray exposure modelling in Provence (south-east France): Earth and Planetary Science Letters, v. 7010, p. 1–21.

Sieh, K., 1996, The repetition of large-earthquake ruptures: Proceedings of the National Academy of Sciences of the United States of America, v. 93, p. 3764–3771, doi: 10.1073/pnas.93.9.3764.

Stone, J.O., 2000, Air pressure and cosmogenic isotope production: Journal of Geophysical Research, v. 105, no. B10, p. 23,753–13,759, doi: 10.1029/2000JB900181.

Tapponnier, P., and Molnar, P., 1979, Active faulting and Cenozoic tectonics of the Tien Shan, Mongolian and Baykal regions: Journal of Geophysical Research, v. 84, p. 3425–3459.

Van der Woerd, J., Ryerson, F.J., Tapponnier, P., Gaudemer, Y., Finkel, R., Meriaux, A.S., Caffee, M.W., Guoguang, Z., and Qunlu, H., 1998, Holocene left-slip rate determined by cosmogenic surface dating on the Xidatan

segment of the Kunlun fault (Qinghai, China): Geology, v. 26, p. 695–698, doi: 10.1130/0091-7613(1998)026<0695:HLSRDB>2.3.CO;2.

Van der Woerd, J., Tapponnier, P., Ryerson, F.J., Meriaux, A.S., Meyer, B., Gaudemer, Y., Finkel, R., Caffee, M.W., Zhao, G.G., and Xu, Z.Q., 2002, Uniform postglacial slip rate along the central 600 km of the Kunlun fault (Tibet), from Al-26, Be-10, and C-14 dating of riser offsets, and climatic origin of the regional morphology: Geophysical Journal International, v. 148, p. 356–388, doi: 10.1046/j.1365-246x.2002.01556.x.

Vassallo, R., Ritz, J-F., Braucher, R., Jolivet, M., Larroque, C., Sue, C., Todbileg, M., Javhaa, D., and Bourlès, D.L., 2004, Timing and uplift rates in Cenozoic transpressional mountain ranges within the Mongolia-Siberia region, RST Strasbourg, September 2004, Abstract RSTGV-A-00210.

Vassallo, R., Ritz, J.-F., Braucher, R., and Carretier, S., 2005, Dating faulted alluvial fans with cosmogenic ^{10}Be in the Gurvan Bogd mountain (Gobi-Altay, Mongolia): Climatic and tectonic implications: Terra Nova, v. 17, p. 278–285, doi: 10.1111/j.1365-3121.2005.00612.x.

Manuscript Accepted by the Society 11 April 2006